Alma Mater Studiorum - Università di Bologna

SCUOLA DI SCIENZE

Dipartimento di Chimica Industriale “Toso Montanari”

Corso di Laurea Magistrale in

Chimica Industriale

Classe LM-71 - Scienze e Tecnologie della Chimica Industriale

Selective oxidation of furfural and 5-methylfurfural under green conditions

Tesi di laurea sperimentale

CANDIDATO

Bruno Reghizzi

RELATORE

Prof. Fabrizio Cavani

CORRELATORE

Dr Robert Wojcieszak

Prof. Sébastien Paul

Anno Accademico 2015-2016

SUMMARY

INTRODUCTION

Bio-renewable fuels and chemicals are becoming increasingly important as humans continue to deplete petroleum resources. An important aim for the future is to develop new processes from biomass and use it as a versatile feedstock because it is the largest carbon resources on earth. The increasing cost of fossil fuels and concerns about their environmental impact are accelerating the transition to a biomass-based economy. While fuel production from biomass has gained much attention, the use of renewable resources is also very important for the production of chemicals. Typically, chemical intermediates have a much higher value than fuels. These intermediates, traditionally derived from fossil fuels, can be further transformed into solvents, polymers, and specialty chemicals [1]. Currently, there is an intensive research on the use of lignocellulosic raw material, because it is a non-eligible biomass, for producing chemical intermediates. Out of an estimated 170 billion metric tons of biomass produced every year, roughly 75% are in the form of carbohydrates which makes biomass carbohydrates the most abundant renewable resource [2].

1 Biorenewable route

Cell walls of plants consist mainly of three organic compounds: cellulose, hemicellulose, and lignin (Figure 1). These compounds are also major components of natural lignocellulosic materials. Cellulose molecules arrange regularly, gather into bundles, and determine the framework of the cell wall. Fibers are filled with hemicellulose and lignin. The structure of the plant cell wall is compact. There is different bonding among cellulose, hemicellulose, and lignin. Cellulose and hemicellulose or lignin molecules are mainly coupled by a hydrogen bond. In addition to the hydrogen bond, there is the chemical bonding between hemicellulose

and lignin, which results in the lignin, isolated from natural lignocelluloses, always contains a small amount of carbohydrates.

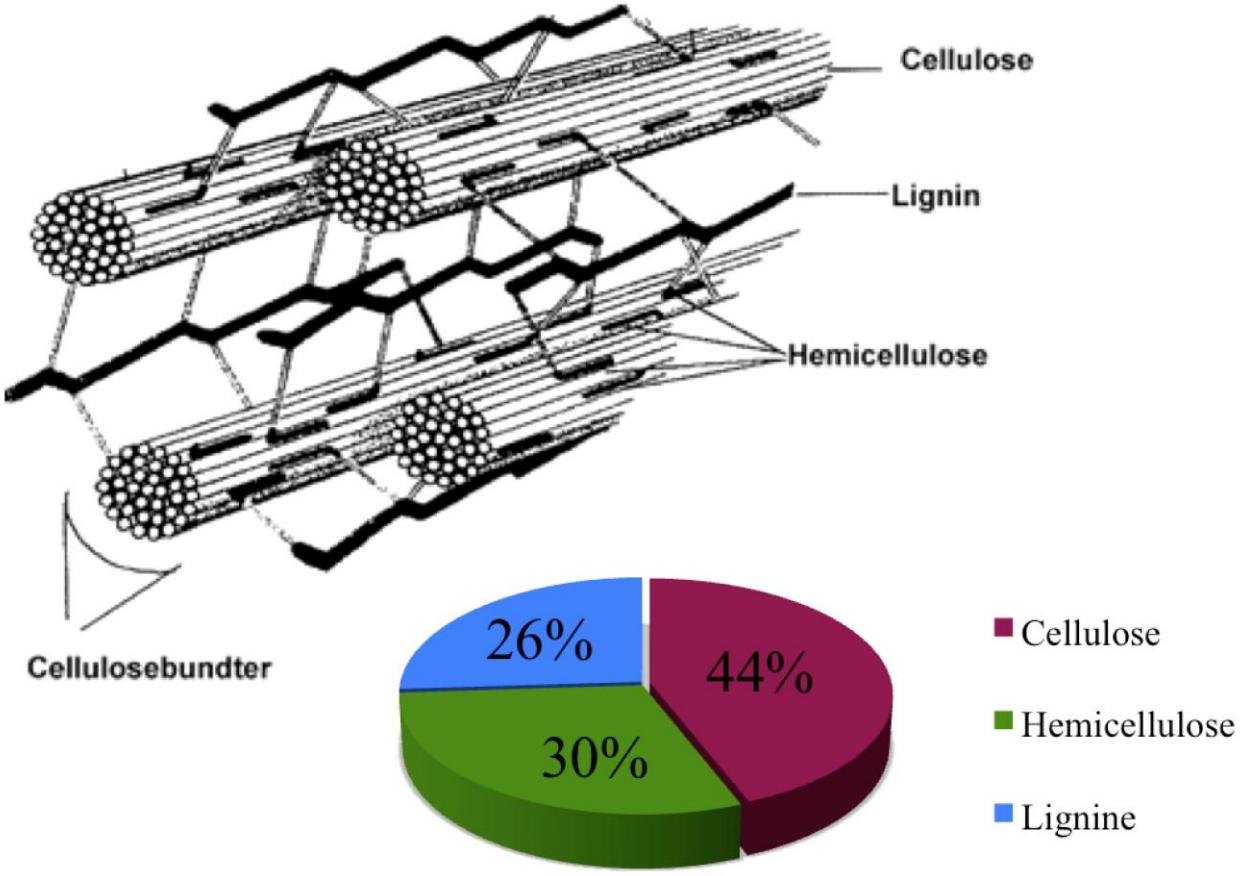

Figure 1. *Secondary cell walls composition*

The chemical bonds between the hemicellulose and lignin mainly refer to the chemical bonds between galactose residues, arabinose residues on the side chains of hemicellulose molecules and lignin, and carbohydrates, with this knowledge gained through research on the separated lignin-carbohydrate complexes (LCCs) [3, 4]. Table 1 shows the chemical composition and structure of cellulose, hemicellulose, and lignin. Cell walls mainly consist of cellulose, hemicellulose, and lignin in a 4:3:3 ratio (Figure 1). This ratio differs from sources such as hardwood, softwood, and herbs. Besides these three components, natural lignocellulosic materials contain a small amount of pectin, nitrogenous compounds, and the secret ash. For instance, the

element content of wood is about 50 % carbon, 6 % hydrogen, 44 % oxygen, and 0.05–0.4 % nitrogen.

Table 1. *Chemical composition of lignin, hemicellulose and cellulose*

	Lignin	Hemicellulose	Cellulose
Subunits	Guaiacylpropane (G), syringylpropane (S), p-hydroxyphenylpropane (H)	D-Xylose, mannose, L-arabinose, galactose, glucuronic acid	D-Pyran glucose units
Bonds between the subunits	Various ether bonds and carbon-carbon bond, mainly β-O-4 ether bond	β-1,4-Glycosidic bonds in main chains; β-1.2-, β-1.3-, β-1.6-glycosidic bonds in side chains	β-1,4-Glycosidic bonds
Polymerization	4,000	Less than 200	Several hundred to tens of thousands
Polymer	G lignin, GS lignin, GSH lignin	Polyxylose, galactoglucomannan (Gal-Glu-Man), glucomannan (Glu-Man)	β-Glucan
Composition	Amorphous, inhomogeneous, nonlinear three-dimensional polymer	Three-dimensional inhomogeneous molecular with a small crystalline region	Three-dimensional linear molecular composed of the crystalline region and the amorphous region
Bonds between three components	Contain chemical bond with hemicellulose	Contains chemical bond with lignin	Without chemical bond

1.1 Cellulose

Cellulose is the most abundant renewable organic resource on Earth and is widespread in higher plants, bacteria, marine algae, and other biomass. The total annual amount of cellulose is several billion tons, revealing the huge economic value of it. Cellulose is the main component of the plant cell. Although some animals (such as tunicates) and some bacteria contain cellulose, the content of cellulose in these species is negligible when compared with plants. Cellulose was first separated by Anselme Payen (1839) from timber, which was alternately treated with nitric acid and sodium hydroxide solution. It is a “-1,4-linked” linear polymer of glucose units and is insoluble in water, dilute acidic solutions, and dilute alkaline solutions at normal

temperatures. Although the structure and composition of the cell walls of plants vary widely, the cellulose content usually accounts for 35–50 % of dry weight and, peculiarly, almost 100 % for cotton. Study of the supramolecular structure of natural cellulose showed that the crystalline and non-crystalline phases intertwine to form the cellulose. The non-crystalline phase (Figure 2) assumes an amorphous state when analyzed by X-ray diffraction because most hydroxyl groups of glucose molecule are amorphous.

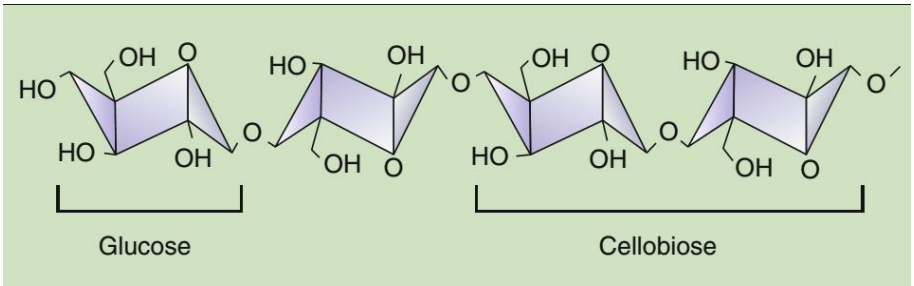

Figure 2. *Non-crystalline structure of cellulose*

However, large amounts of hydroxyl groups in the crystalline phase form many hydrogen bonds, and these hydrogen bonds construct a huge network that directly contributes to the compact crystal structure [5]. In most conditions, the cellulose is wrapped by hemicellulose (dry matter accounting for 20–35 %) and lignin (dry matter accounting for 5–30 %). Cellulose has become an important raw material for the pulp and paper, textile, and fibrous chemical industries. Predictably, bioenergy generated from lignocellulosic materials will become clean energy in the future.

1.2 Hemicellulose

Hemicellulose is another main component of plant fiber materials. In 1891, Schulz [6] thought that polysaccharides that easily separated from plant tissue were semi-finished products of cellulose or precursor molecules of cellulose. They were called hemicellulose. He also found that this component easily hydrolyzed to monosaccharides in hot, dilute mineral acid or cold 5 % NaOH solution. The chemical structure and biological function of hemicellulose remained non-clear for several decencies. In recent years, more information about hemicellulose were

obtained due to improvements in polysaccharide purification as well as application of various types of chromatography, spectroscopy, nuclear magnetic resonance, mass spectrometry (MS), and electron microscopy. In 1962 Aspinall defined that hemicellulose was derived from polysaccharides of plants and included the basic chain containing residues of D-xylose, D-mannose, D-glucose, or D-galactose and other glycosyls as branched chains linked to this basic chain. The purification of hemicelluloses was conducted according to the different alkaline solubility if compared with that of cellulose. In 1978, Whistler claimed that hemicellulose was the polysaccharide extracted by an alkali solution, except cellulose and pectin. Unlike cellulose, hemicellulose is indeed, a copolymer composed of different amounts of several saccharide molecules [7].

1.3 Lignin

Lignin is the second most abundant organic polymers in plants, just behind cellulose. It is the exclusive chemical composition of gymnosperm and angiosperm. The content of lignin in woods and gramineaes is about 20–40% and 15–20 %, respectively. Lignin is the general name of a group of phenol-like compounds called lignols. Their inhomogeneity is manifested in different species of plants, length of growing season, and different parts of the plants. Even in different morphologies of cells of the same xylem or different cell wall layers, the structures of lignin are not the same [8]. Lignin is a complex polymer composed of phenylpropane units nonlinearly and randomly linked. Three main monomers are coumaryl alcohol, coniferyl alcohol, and sinapyl alcohol (Figure 3).

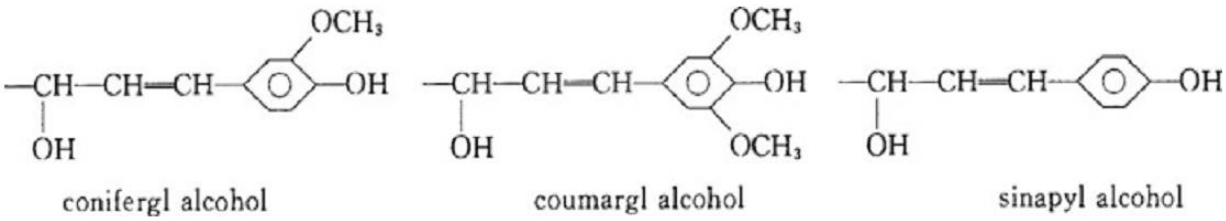

Figure 3. *Basic structural unit of lignin*

Because of the different monomers, lignin can be divided into three types (Fig. 3): i) syringyl lignin polymerized by syringyl propane, ii) guaiacyl lignin polymerized by guaiacyl propane, and iii) hydroxy-phenyl lignin polymerized by hydroxy-phenyl propane. Usually, gymnosperm mainly contains guaiacyl (G) lignin; the dicotyledon mainly contains guaiacyl-syringyl (GS) lignin and the monocotyledon mainly contains guaiacyl-syringyl-hydroxy-phenyl (GSH) lignin [9]. Generally, lignin in plant is divided into softwood, hardwood, and grass lignins. Based on the structure of lignin, Gibbs divided lignin into G lignin and GS lignin. G lignin is chiefly formed through dehydrated oligomerization of coniferyl alcohol, and its structure is homogeneous. This kind of lignin gives negative result of Maule reaction because less than 1.5 % of syringaldehyde and about 5 % of p-hydroxybenzaldehyde are generated when oxidized by nitrobenzene. Most lignin in softwood belongs to G lignin, which is copolymerized by guaiacyl and gives positive result of Maule reaction [10].

2 Furfural

The aim of this work is to investigate the catalytic transformation of furfural and 5-methyl furfural, two important intermediates obtained from biomass upgrading. It is more particular focused on their oxidation using green conditions and heterogeneous catalysts. In literature many processes for the catalytic oxidation of furfural are reported. In this process the highly desired product is maleic acid (MA), but many other interesting products like furoic acid and furanone can be also obtained depending on the catalytic system used (and/or conditions). Unfortunately, very often this type of reaction hides several problems and specific conditions must be applied to improve furfural conversion, overall carbon balance, yield and selectivity to the desired products.

Furfural is a heterocyclic aldehyde, with the ring structure shown in Figure 4. Its chemical formula is OC_4H_3CHO. It is a colorless oily liquid with the odor of almonds, which quickly darkens when exposed to air due to the decomposition.

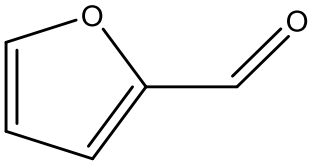

Figure 4. *Schematic representation of furfural molecule*

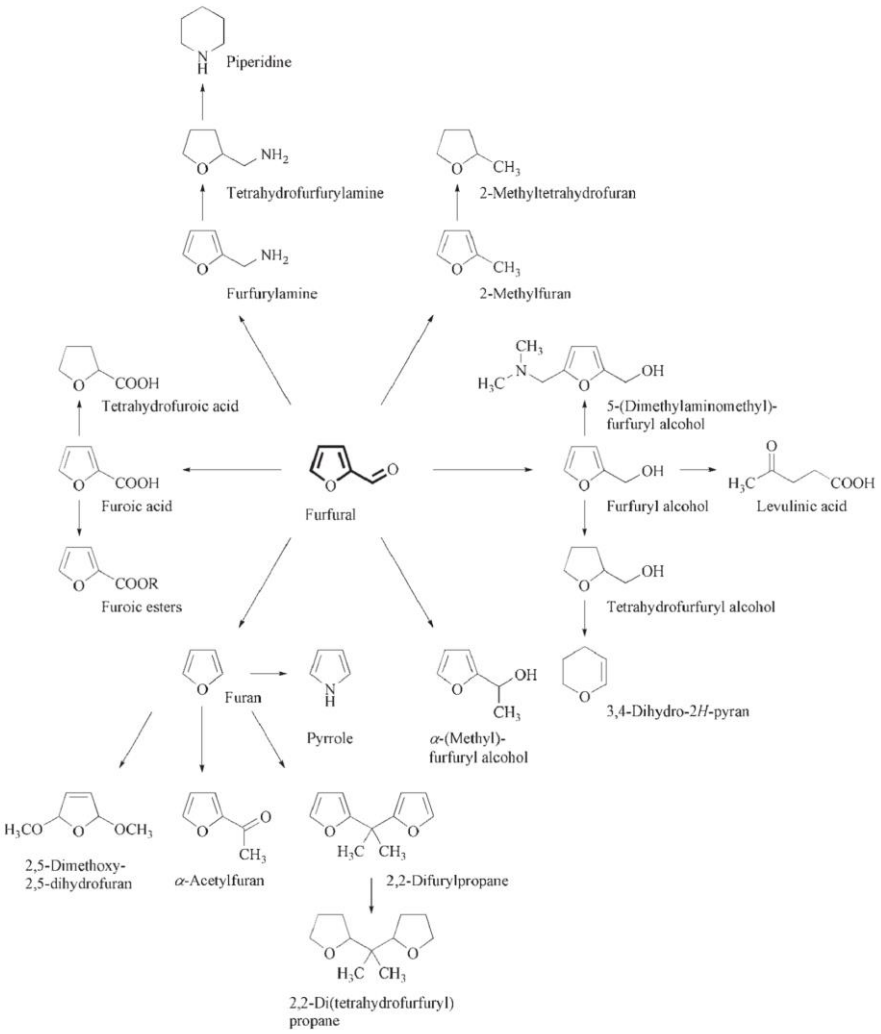

Scheme 1. Chemicals derived from furfural

Figure 5. *Different products obtained from furfural upgrading [11]*

2.1 Furfural proprieties and security information

Table 2. *Physical and technical properties of furfural [11]*

PHYSICAL DATA	
mpg	−36 °C(lit.)
bp	54-56 °C11 mm Hg
density	1.16 g/mL at 25 °C(lit.)
vapor density	3.31 (vs air)
vapor pressure	13.5 mm Hg (55 °C)
refractive index	n20/D 1.527
FEMA	2489
Fp	137 °F
storage temp	2-8°C
color	very deep brown
Water Solubility	8.3 g/100 mL
FreezingPoint	-36.5℃
Sensitive	Air Sensitive
Merck	14,4304
BRN	105755
Stability	Stable. Substances to be avoided include strong bases, strong oxidizing agents and strong acids. Flammable.
CAS DataBase Reference	98-01-1(CAS DataBase Reference)
NIST Chemistry Reference	2-Furancarboxaldehyde(98-01-1)
EPA Substance Registry System	2-Furancarboxaldehyde(98-01-1)

SAFETY	
Hazard Codes	T,Xi
Risk Statements	21-23/25-36/37-40-36/37/38
Safety Statements	26-36/37/39-45-1/2-36/37
RIDADR	UN 1199 6.1/PG 2
WGK Germany	2
RTECS	LT7000000
F	1-8-10
Hazard Note	Irritant
HazardClass	6.1
PackingGroup	II
Hazardous Substances Data	98-01-1(Hazardous Substances Data)

2.2 Furfural synthesis

All plants contain hemicellulose, a polymer formed by five carbon atoms sugars. When heated with sulfuric acid, hemicellulose undergoes hydrolysis to yield C5 sugars, principally xylose. Under the same conditions of heat and acid, xylose and other five carbon sugars undergo dehydration, losing three molecules of water to form furfural as shown in Figure 6 [11].

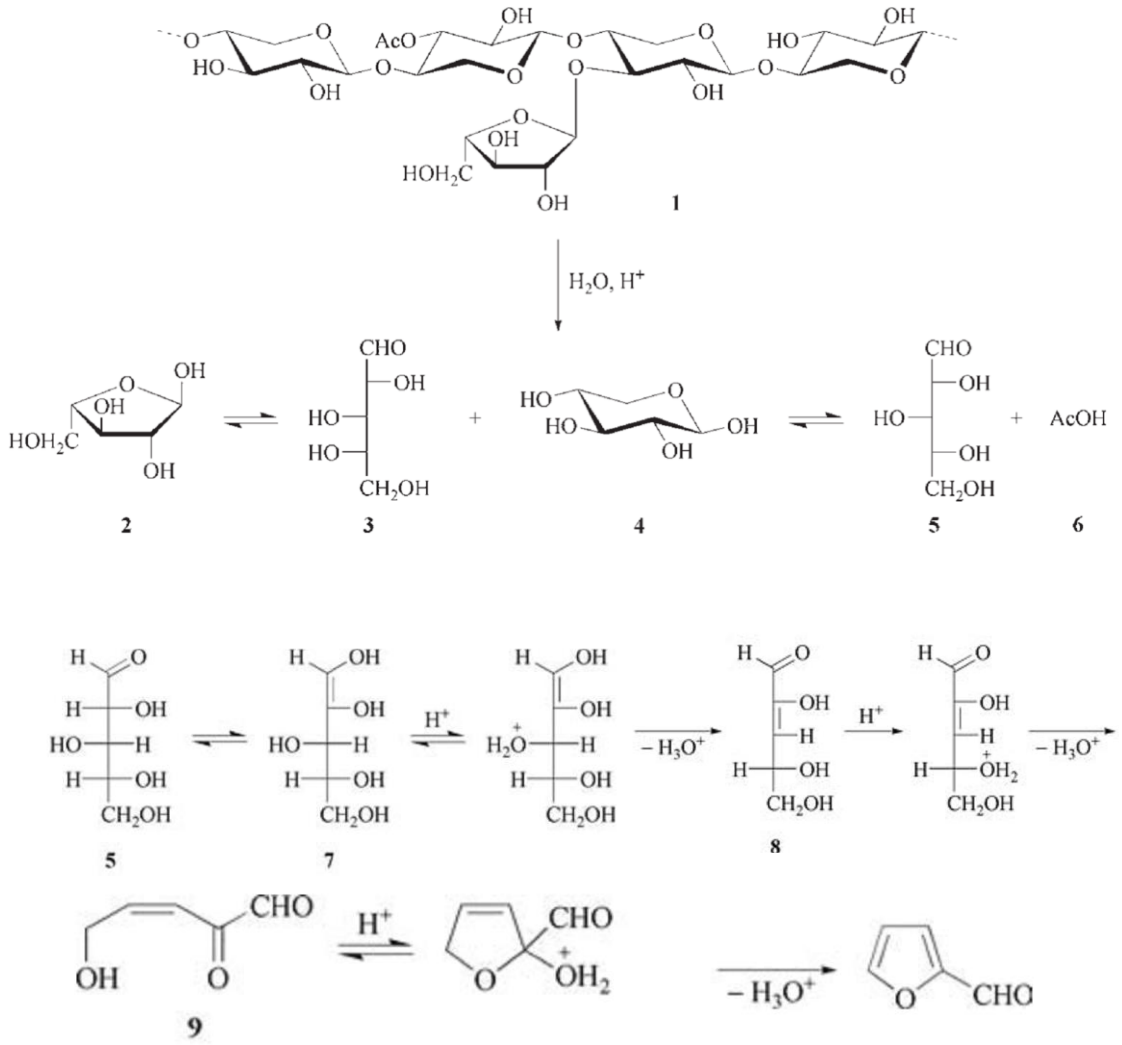

Figure 6. *(1) arabinoxylans; (2) L-arabinofuranose; (3) L-arabinose; (4) Xylopyranose; (5) D-Xylose; (6) Carboxylic acids; (7) 1,2-enediol form of xylose; (8) 3-deoxy-D-xylosulose; (9) 3,4-dideoxy-D-xylo-3-pentenosulose*

For crop residue feedstocks, between 3% and 10% of the mass of the original plant matter can be recovered as furfural, depending on the type of the feedstock. Furfural and water evaporate together from the reaction mixture, and separate upon condensation. The global production capacity of furfural is about 800,000 tons (data from 2012). China is the biggest furfural producer, and supplies the most important part of global consumption. The other two major commercial producers are Illovo Sugar in the Republic of South Africa and Central Romana in the Dominican Republic.

On the laboratory scale, synthesis of furfural from corncobs takes place by reflux with dilute sulfuric acid [11]. The lignocellulosic residue that remains after the removal of the furfural is used to generate all the steam requirements of the furfural plant. Moreover more energy efficient plants have excess residue, which can be used for co-generation of electricity, cattle feed, activated carbon, mulch/fertilizer, etc.. It also has been used as a glue extender in the North American board industry [12].

2.3 Furfural applications

Furfural is an important intermediate in chemical industry. It is used as a solvent, for the production of solid resins and as an intermediate for the synthesis of other compounds. It can been also catalytically oxidized with O_2 or H_2O_2 to form maleic acid, maleic anhydride (in a non-aqueous solvent), 2(5H)furanone and furoic acid. The synthesis of furoic and maleic acids will be studied in details during this work. For implement of this process the information obtained during past studies [13] will be used.

2.4 Products of furfural oxidation

2.4.1 Maleic acid:

Maleic acid (MA) is a very important chemical intermediate that find applications in many different fields of industrial chemistry. MA is an important raw material used in the manufacture of lubricant additives, unsaturated polyester resins, surface coatings, plasticizers, copolymers and agricultural chemicals. MA is a dicarboxylic acid that leads to succinic acid by hydrogenation. Historically, MA was firstly prepared in 1830 but its commercial manufacture did not begin until almost a century later.

MA can be commercially produced by the vapor-phase oxidation of benzene or butane/butane using O_2 oxidation. This reaction is very exothermic and produces a lot of CO and CO_2. The quest for sustainable and environmentally benign sources of energy and, more recently, of chemicals has attracted much attention in the recent

years. The production from biomass seems an ideal solution and biomass-derived platform molecules, such as maleic acid, fumaric acid or maleic anhydride have been identified as top value added chemicals [7].

A reaction mechanism for the production of MA from furfural is proposed following Figure 7.

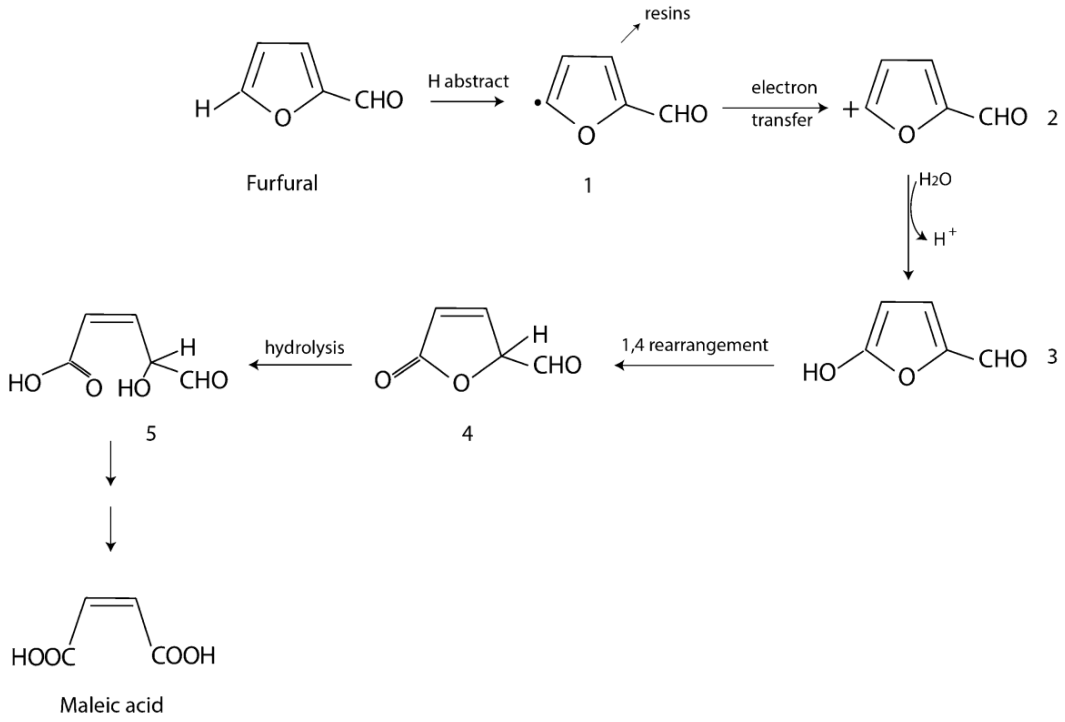

Figure 7. *Reaction mechanism of maleic acid synthesis[14]*

2.4.2 2-Furoic acid:

2-Furoic acid (FA) is a preservative, acting as a bactericide and fungicide. It is also considered as an acceptable flavoring ingredient and is generally recognized as safe (GRAS) since 1995 by the Flavor and Extract Manufacturers Association (FEMA). 2-Furoic acid is characterized as a colorless liquid and has a distinct odor described in the Encyclopedia of Food and Color Additives as sweet, oily, herbaceous, and earthy [2]. FA is often used as a starting material for the production of furoate esters. FA and its derivatives are also used in the production of nylons principally applied in biomedical researches. There are also several work on develop the use of FA in the field of optical technology.

2.4.3 2-(5H)-furanone:

2-(5H)-furanone, also known as γ-crotonolactone (GCL), is a heterocyclic organic compound. Classified as a lactone, this colorless liquid is often called "butenolide." As a class of compounds, substituted derivatives, which are not in fact prepared from the parent 2-furanone, are called butenolides.

3 5-methylfurfural

5-methylfurfural is a heterocyclic aldehyde, with the ring structure shown in Figure 7. Its chemical formula is OC_5H_2CHO. It is a deep yellow to brown oily liquid, sensitive to air.

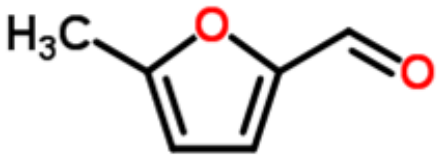

Figure 8. *Schematic representation of the 5-methylfurfural molecule.*

3.1 5-methylfurfural proprieties:

Table 3. Physical and technical properties of 5-methylfurfural

PHYSICAL DATA	
bp	187-189 °C(lit.)
density	1.107 g/mL at 25 °C(lit.)
refractive index	n20/D 1.531
FEMA	2702
Fp	163 °F
storage temp.	Refrigerator
color	very deep yellow to brown
Sensitive	Air Sensitive

SAFETY	
Hazard Codes	Xi
Risk Statements	36/37/38
Safety Statements	26-36-24/25
WGK Germany	2
RTECS	LT7032500
HS Code	29329995

3.2 5-Methylfurfural synthesis:

The large-scale industrial production of MF involves 5-methylfuran, N,N-dimethylformamide, and phosphorus oxychloride or phosgene. During this process, significant excesses of expensive and strongly poisonous phosphorus oxychloride and N,N-dimethylformamide are used.

Another reported method to produce MF starts from biomass-derived carbohydrates (hexoses) *via* a two-step process. First, 5-chloromethylfurfural (CMF) is obtained by acidic decomposition of carbohydrates in high concentrations of chloride ion. MF is then obtained by hydrogenation of CMF with palladium as catalyst under an atmosphere of hydrogen. The yield of the hydrogenation step is up to 98 % [16]. However, CMF formation from hexoses (such as fructose) requires long reaction times (ca. 10h) and large quantities of organic solvent and surfactants, making the process commercially unattractive. Very recently, Mascal and Nikitin have improved the CMF synthesis step by demonstrating that not only fructose and glucose, but also cellulose and even raw biomass can be converted into CMF in good yields (ca. 70–80 %). The procedure still requires a relatively large amount of organic solvents [1].

3.3 5-Methylfurfural applications:

5-Methylfurfural is a useful intermediate for the production of pharmaceuticals, chemicals for agriculture, perfumes, and other applications. It is also a common

flavoring component in the food industry, and is even considered a potential anti-tumor agent [10].

3.4 Product of 5-methylfurfural oxidation

The only significant product researched from 5-methyl furfural oxidation is 5-methyl-2-furoic acid. This product is an emerging molecule used as an additive in many different fields like food, colors and, most important, it can be used as a fuel additive in gasoline, diesel, jet fuel etc… because it improves the performances of spark ignition internal combustion engines and compression ignition internal combustion engines. In addition, testing shows indications that 5-methyl-2-furoic acid could improve performances of air breathing engines as well [17].

4 Biphasic system

Furfural, in oxidizing atmosphere, under high pressure and at high temperature, tends to polymerize and undergoes degradation in aqueous environment. To avoid this trend, Guo and Yin [1] performed the reaction of furfural oxidation in a biphasic aqueous/organic medium. The main reaction takes place in the aqueous phase and the organic phase plays the role of a reservoir, which gradually releases furfural through phase equilibrium. The biphasic system had improved the yield to the desired products like MA, FA and furanone and, at the same time, the conversion of furfural had been decreased, improving the carbon balance and the selectivity of the reaction. The co-solvent chosen for the tests was MIBK (Methyl Iso-Butyl Ketone), which is usually used in the HMF (HydroxyMethylFurfural) extraction, and has good proprieties to form a water/organic biphasic system. There are many other organic solvents, which can be used. As appeared from the literature several tests with: nitrobenzene, tetrachloromethane, toluene, nitromethane, p-xylene, cyclohexane, tetradecane and tetrachloroethane have been already performed. Each of them shows different conversion and different yields, meaning that the solvent has a huge impact on the activity of the reagents. It is also very important to chose a good ratio between

water and organic solvent. Indeed, high water to organic solvent ratio gives good results in terms of the conversion because the reaction occurs in aqueous phase but at the same time it also decreases the overall carbon balance of the reaction. On the contrary, an increase of the quantity of organic solvent will cause increase of the selectivity to desired products but with a lower conversion of the furfural [1].

5 *Heterogeneous catalysts used for furfural oxidation*

From the industrial point of view the oxidation of furfural needs active, selective and stable heterogeneous catalysts. There are many publications that deal with this topic presenting more or less interesting results. There is a lot of advantages in use of heterogeneous catalysts. Indeed, solid catalyst can be easily removed at the end of the reaction, by a simple filtration and can be recovered or wasted with a small additional cost. Homogeneous catalysts have to be separated using expensive treatments which, from the economical point of view, is not adequate for the industrial applications. However, due to the different mechanisms of oxidation, solid catalysts are less active then the homogeneous ones and need a high level of optimization to be suitable for the industrial use. Moreover, the leaching of active phase needs to be controled and this requires a lot of tests and use of advanced catalysts. Many publications studied various types of heteropolyacids and, in particular, phosphomolibdic acids. Some authors studied also the influence of the nature of counter-ions of the copper (II) cation, which could modulate the redox proprieties of the Cu^{2+} [18]. It was found that the acetate, sulfate and nitrate counterparts could significantly improve the yield of maleic acid in the oxidation of furfural. In contrast, using the chloride anion does not improve the activity, and using carbonate even leads to a detrimental effect on catalytic activity [19]. However, it was shown that the extra addition of nitrate to the reaction mixture did not improve the catalytic activity at all, which suggests that the nitrate anion does not promote the conversion of furfural to maleic acid directly. It may play the role of modulator of the redox efficiency [19].

Very interesting results were observed in the case of the combination of copper nitrate with phosphomolybdic acid. The mixture of these two reagents yielded in enhancement of the activity in the furfural oxidation to maleic acid. For a mixture of 0.8 mmol of phosphomolybdic acid and 0.4 mmol of copper nitrate, the yield of maleic acid could be improved up to 49.2% with a selectivity of 51.7%, and the conversion of furfural was 95.2% (as compared to the test without $Cu(NO_3)_2$: 38.4, 43.3 and 88.7%, respectively) [19]. Several tests were also made with transition metals complexes such as $FeSO_4$, $CuSO_4$, $Mn(acac)_2$, $MoO_2(acac)_2$, $Co(acac)_2$ and $Co(OAc)_2$. All of them were studied in the same conditions were found less effective for catalytic oxidation of HMF into MA, and the yield of MA was lower than 2% [19].

Quite similar results were observed in the oxidation of furfural in the presence of redox metal salt catalysts [19]. It was shown that copper acetate and iron sulfate enabled respectively 18.6 and 12.1% yields in the expected maleic acid. On the other hand, the catalysts based on other metal such as $Mn(OAc)_2$, $RuCl_3$ and $NiCl_2$ were substantially less efficient for maleic acid formation. Interestingly, a $Pd(OAc)_2$ catalyst showed a 15.9% yield to furoic acid, while only traces of this compound were observed over other metal catalysts. The summary of the catalytic results obtained in liquid phase are presented in Table 4.

Table 4. *Literature review on liquid phase oxidation of Furfural and HMF [1]*

CATALYST	CONDITIONS	FURFURAL or HMF CONVERSION	MA yield	MA selectivity
$H_3PMo_{12}O_{40}$	383 K, O_2 20 bar, H_2O + nitrobenzene	67 (furfural)	38	56
$H_3PMo_{12}O_{40}$	383 K, O_2 20 bar, H_2O + toluene	73 (furfural)	37	50

CATALYST	CONDITIONS	FURFURAL or HMF CONVERSION	MA yield	MA selectivity
$H_3PMo_{12}O_{40}$	383 K, O_2 20 bar, H_2O + *p*-xylene	66 (furfural)	35	53
$H_3PMo_{12}O_{40}$	383 K, O_2 20 bar, H_2O + cyclohexane	85 (furfural)	38	45
$H_3PMo_{12}O_{40}$	383 K, O_2 20 bar, H_2O + tetradecane	82 (furfural)	38	46
$H_3PMo_{12}O_{40}$	383 K, O_2 20 bar, H_2O	86 (Furfural)	38	44
$VO(acac)^2$	363 K, O_2 10 bar, CH_3CN	99 (HMF)	52	52
Amberlyst 15	353 K, H_2O_2, H_2O, 24 h	99 (furfural)	11	11
Nafion NR50	353 K, H_2O_2, H_2O, 24 h	99 (furfural)	11	11
Nb_2O_5	353 K, H_2O_2, H_2O, 24 h	99 (furfural)	4	5
ZrO_2	353 K, H_2O_2, H_2O, 24 h	99 (furfural)	5	5
$H_6PV_3MO_9O_{40}$	383 K, O_2 20 bar, CH_3CN	99 (furfural)	12	12

CATALYST	CONDITIONS	FURFURAL or HMF CONVERSION	MA yield	MA selectivity
$VO(acac)^2$	363 K, O_2 10 bar, DMF	96 (HMF)	7	7
$H_5PV_2Mo_{10}O_{40}$ + $Pd(OAc)_2$(1/1)	383 K, O_2 20 bar, CH_3CN	94 (furfural)	14	15
$VO(acac)^2$	363 K, O_2 10 bar, TFT	96 (HMF)	7	7
$VO(acac)^2$	363 K, O_2 10 bar, CH_2Cl_2	99 (HMF)	16	16
$VOSO_4$	363 K, O_2 10 bar, CH_3CN	NC (furfural)	34	NC
$Co(OAc)_2$	363 K, O_2 10 bar, CH_3CN	NC (furfural)	2	NC
$Co(NO_3)_2$	371 K, O_2 20 bar, H_2O	69 (furfural)	4	6
$FeSO_4$	371 K, O_2 20 bar, H_2O	90 (furfural)	12	13
V_2O_5	371 K, O_2 20 bar, H_2O	72 (Furfural)	6	8
$CuSO_4$	371 K, O_2 20 bar, H_2O	67 (furfural)	19	29

CATALYST	CONDITIONS	FURFURAL or HMF CONVERSION	MA yield	MA selectivity
$Cu(NO_3)_2$	371 K, O_2 20 bar, H_2O	86 (furfural)	24	28
$Cu(OAc)_2$	371 K, O_2 20 bar, H_2O	71 (furfural)	19	26
$H_3PMo_{12}O_{40}$ + Cu$(NO_3)_2$(2/1)	371 K, O_2 20 bar, H_2O	95 (furfural)	49	52

5.1 Gold nanoparticles

The study of gold-based catalysts has grown significantly in recent years following the demonstration that their activity increases significantly when used in the form of nanoscale particles. This was especially well demonstrated for oxidation of renewable biomass-carbohydrates in general, and sugars in particular. Gold catalysts were found to have a clear advantage in activity and selectivity compared to platinum- and palladium-based catalysts used so far for carbohydrate oxidation. Due to the total selectivity of gold catalysts, expensive purification processes as in biotechnological processes are not necessary. A unique property of gold catalyst was found by varying the aldose (e.g., glucose, lactose, maltose, xylose, arabinose): the same gold catalyst is able to completely convert all different aldoses to their corresponding aldonic acids. Such universality in carbohydrate oxidation was previously unknown for chemical as well as biocatalysts. By applying gold catalysts for other carbohydrates oxidation, many interesting products can be obtained. It was found that unsupported gold particles in aqueous solution (average diameter: 3–5 nm) show a surprisingly high activity in the aerobic oxidation of glucose, not far from that of enzymatic

systems [20-21]. Moreover, a linear correlation between activity and number of exposed gold atoms was demonstrated [21]. In 2002, Biella et al. [22] reported in their paper that gold colloids immobilized on carbon are dramatically more active for catalytic glucose oxidation and exhibit a superior 100% selectivity towards sodium gluconate. Even though these systems are very active and selective, the catalysts described by Biella do not have a sufficient long-term stability as the activity decreases about 50% within only four repeated batches [22-23]. Similarly prepared gold colloids supported on carbon and their kinetics in glucose oxidation were studied by Önal et al. [24]. Although Önal reported a lower selectivity, in general, the superior performance of the gold catalysts in terms of activity has been confirmed. Catalytic activity inversely proportional to the diameter in the size range of 2.5–6nm and a sudden loss of activity above 10nm in size were observed. The stability of the colloid particles was low, coagulation occurred after about 400 s [21-25]. To improve the stability, gold colloids were deposited on carbon support. The initial rates of the reaction were unchanged compared to the rates observed with nonsupported particles operated under the same conditions, hence it was concluded that the support is of limited importance in the origin of the catalyst activity in the oxidation of glucose. However the gold–support interaction was declared to be essential for the formation of a stable catalyst system [26-27]. On the contrary other authors [24] reported different catalytic activity using different type of carbon supports with the same Au particle size indicating a specific metal–support interaction. Ishida et al. observed that gold particle size influences the catalytic effect more significantly than the nature of the support comparing carbon and different metal oxide supports such as Al_2O_3, ZrO_2, TiO_2, CeO_2 [28-29].The gold, in fact, is not a metal active from a catalytic point of view if used as a bulk material because of its low tendency to chemisorption due to its electronic configuration of $5d^{10}6s^1$ type. The chemical adsorption on a transition metal is made possible by the interaction of the HOMO and LUMO orbitals. From the catalytic point of view, the force of the chemical adsorption must be sufficiently strong to allow an effective interaction, but not too much, otherwise,

an excessive retention of the molecule to the metal surface, would reduce the activity. Because of $5d^{10}6s^{1}$ electronic configuration, when a molecule adsorbs on metallic gold bulk surface, a strong effect of back bounding to the antibonding orbital is observed. A very weak interaction with the adsorbate does not allow a correct activation. Gold nanoparticles are used in a large range of applications, including the biomedical monitoring, cosmetics, and lubricants. The most important are listed below.

5.1.1 Gold nanoparticles principal uses

Electronics - Gold nanoparticles are designed for use as conductors from printable inks to electronic chips. As the world of electronics become smaller, nanoparticles are important components in the chip design [30]. Nanoscale gold nanoparticles are being used to connect resistors, conductors, and other elements of an electronic chip.

Photodynamic Therapy - Near-IR absorbing gold nanoparticles (including gold nanoshells and nanorods) produce heat when excited by light at wavelengths from 700 to 800 nm. This enables these nanoparticles to eradicate targeted tumors [31]. When light is applied to a tumor containing gold nanoparticles, the particles rapidly heat up, killing tumor cells in a treatment also known as hyperthermia therapy.

Therapeutic Agent Delivery - Therapeutic agents can also be coated onto the surface of gold nanoparticles [32]. The large surface area-to-volume ratio of gold nanoparticles enables their surface to be coated with hundreds of molecules (including therapeutics, targeting agents, and anti-fouling polymers).

Sensors - Gold nanoparticles are used in a variety of sensors. For example, a colorimetric sensor based on gold nanoparticles can identify if foods are suitable for consumption [16]. Other methods, such as surface enhanced Raman spectroscopy, exploit gold nanoparticles as substrates to enable the measurement of vibrational energies of chemical bonds. This strategy could also be used for the detection of proteins, pollutants, and other molecules label-free.

Probes - Gold nanoparticles also scatter light and can produce an array of interesting colors under dark-field microscopy. The scattered colors of gold nanoparticles are

currently used for biological imaging applications [33]. Also, gold nanoparticles are relatively dense, making them useful as probes for transmission electron microscopy. **Diagnostics -** Gold nanoparticles are also used to detect biomarkers in the diagnosis of heart diseases, cancers, and infectious agents [34]. They are also common in lateral flow immunoassays, a common household example being the home pregnancy test. **Catalysis -** Gold nanoparticles are used as catalysts in a number of chemical reactions [35]. The surface of a gold nanoparticle can be used for selective oxidation or in certain cases the surface can reduce a reaction (nitrogen oxides). Gold nanoparticles are being developed for fuel cell applications. These technologies would be useful in the automotive and display industry.

5.1.2 Supports for gold nanoparticles

The support plays a crucial role of dispersing the active phase, to stabilize it in the desired state, to preserve its properties during the chemical reaction and the treatments to which the catalyst will be subjected. The main features are: high thermal stability, high surface area, and good mechanical properties. Non-supported gold nanoparticles have a very high surface energy so they are easy to agglomerate. Therefore, they should be dispersed on a suitable support in order to maintain their stability and catalytic activity. Gold nanoparticles should have good wetting capability and should interact with the high surface area support. AuNPs can be supported on metal oxides, activated carbon, zeolite and other supports by different methods of preparation including impregnation, precipitation, sol-immobilization or microemulsion. Whether the support itself has a catalytic ability, oxide supports are divided into active supports, such as Fe_2O_3, TiO_2, Co_3O_4, etc, and inert supports, like MgO, Al_2O_3 and SiO_2. For Au catalysts supported on active materials, the dominant reaction pathway involves adsorption of a mobile, molecular oxygen species on the support, dissociation at the interface, which supply with reactive oxygen. While for Au supported on inert materials, where the oxygen supply most likely precedes via direct dissociative adsorption on the Au particles, the size of the latter plays a decisive role. In other way, the impact of support on the catalytic activity also

depends on the type of catalyzed reaction. Ishida *et al.* [36] reviewed the impact of supported gold catalyst on the catalytic oxidation of carbohydrates. The study found that compared to the gas phase catalytic oxidation reaction (oxidation of H_2, CO), in the glucose oxidation, the influence of AuNPs' size is much larger than the kind of support in the catalytic activity. Therefore, when using supported gold catalyst to catalyze the glucose oxidation reaction, after choosing suitable support, more attention should be paid to the influence of preparation method on AuNPs' size.

In industrial projects is preferred to support the active phase on metal oxides. Thus the choose of the right support and of the adequate percentage of gold to apply is a very delicate and complex process.

In this work we will study several types of support for gold nanoparticles: hydrotalcite, VPP, ZrO_2 and mixed oxide ZrO_2/HT.

5.2 Hydrotalcite

Several publications reported the oxidative transesterification of furfural using Au NPs supported on basic supports such as hydroxyapatite or hydrotalcite. It is known also that, to avoid the strong adsorption of products on the catalysts surface, the alkaline medium is necessary. However, it could be possible to change the basicity of the catalysts surface without changing the overall pH of the reactant solution. To this purpose Au supported on hydrotalcite was synthetized as reported below.

5.3 Zirconia

One of the most important parameters in catalysis by metals is the dispersion of active phase. ZrO_2 used in our study is a low surface area oxide (Sigma Aldrich). It is known that higher dispersions could be obtained using high surface area supports. For this purpose, the synthesis of the mesoporous zirconium oxide, using an organic template was performed, in order to increase its surface area. The ZrO_2 oxide was prepared as described in [37].

5.4 VPO & VPP

Catalysts based on Vanadium Phosphorus Oxides (VPO) are well known compounds studied and used in particular for the selective oxidation of n-butane to maleic anhydride.

The particular multifunctionality of this catalyst is due to the presence of both redox and acid sites, which can make it suitable for the activation of furfural/5-methyl furfural, following the aim of a deeper investigation in their reactivity.

Due to the difficulty to reproduce in laboratory the industrial catalyst, used for the synthesis of maleic anhydride from n-butane, a sample of industrial prepared $(VO)_2P_2O_7$ (VPP) catalyst was provided from DuPont company.

EXPERIMENTAL PART

6 Methods and calculations

During this thesis the oxidation of furfural and 5-methylfurfural was studied. At the beginning some biphasic systems were tried, then the research was focalized more on the catalysts and on the operating conditions.

6.1 Calculations

The conversion (X) expresses the real part of the reagent that actually is converted during the reaction. It is expressed as follow:

$$X = 100 * [n(t_0) - n(t_f)] / n(t_0)$$

where $n(t_0)$ and $n(t_f)$ are the number of moles of reagent at the t_0 and at the end of the reaction t_f respectively.

The yield (Y) is calculated with the quantity of product obtained during the reaction. It is expressed as follows:

$$Y = 100 * n_{prod}(t_f) / n_{reag}(t_0)$$

where n_{prod} and n_{reag} are number of moles of product and of the substrate respectively.

The selectivity (S) represents the relationship between yield (Y) and conversion (C) to a given product. It is expressed as follow:

$$S = 100 * Y / X$$

The carbon balance (C%) is a parameter less frequently used than the others described above but it is one of the most important. Without the C% it is not possible to obtain correct results of conversion and selectivity and have a good idea about the possible degradation of the products. It is calculated as follows:

$$C\% = C_{prod}(t_f) / [C_{reag}(t_f) - C_{reag}(t_0)]$$

where C_{prod} and C_{reag} are the number of moles of carbon in the reactor before (t_0) and after a test t($_f$).

6.2 Instruments

Many different instruments were used during the project for both qualitative and quantitative results. The reactions were conducted in a semibatch reactor and the synthesized catalysts were characterized. Starting and final solutions from the catalytic tests were analyzed in order to study possible catalyst leaching.

6.2.1 Bench scale reactor

The TOPIndustry Autoclave reactor was used (Figure 9). This autoclave is equipped with high precision heating system and mechanical stirring. This reactor permits to perform catalytic tests up to 250°C and 100 bar.

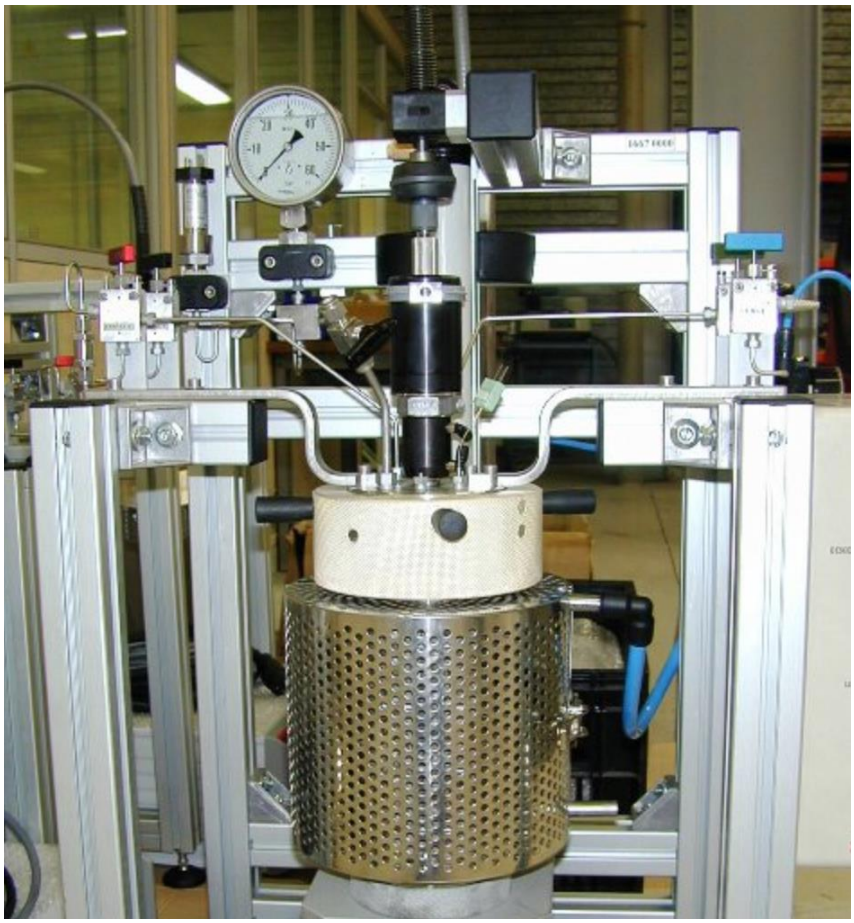

Figure 9. *TOPIndustry autoclave reactor*

Liquid reagents (with or without solvent) are insert in the chamber of the autoclave of the maximal volume of 30 mL. A flow system permits to introduce oxygen to the reactor. There is also an heating system, a mechanical stirrer and a pressure controller. Temperature and stirring are controlled by an external electronic device. Technical scheme of the reactor is given in Figure 10.

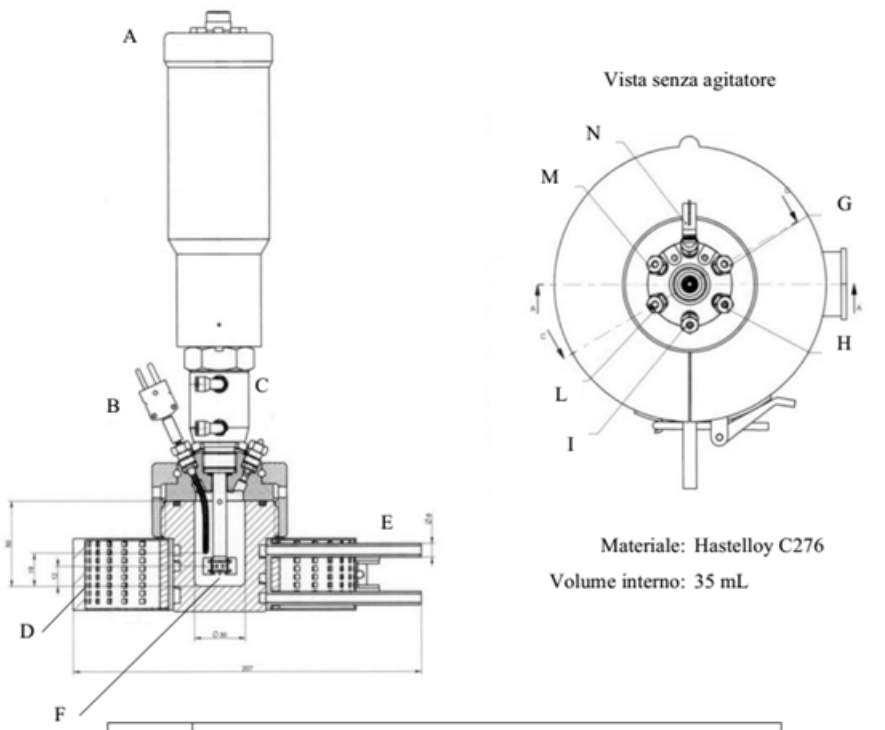

A	coupled magnetic stirrer
B	thermocouple
C	cooling system of the stirrer
D	heating system of the autoclave
E	compressed air cooling system of the autoclave
F	Rushton turbine
G	vent purge
H, I	stoppers
L	sampling valve
M	gas arriving container
N	termocouple

Figure 10. *TOPIndustry autoclave reactor scheme*

6.2.2 Reactor settings & conditions

The reactor was used in batch conditions with the autoclave linked to the oxygen bottle.

The reactant solution is made by the addition of a precise amount of organic substrate (furfural or 5-methylfurfural) with an appropriate solvent for a total volume of 10 mL. Then the mixture is stirred to solubilize completely furfural and 5-methylfurfural. Then 1mL of the solution is taken for HPLC analysis and other 10 ml of water is added to the solution in the reactor. The autoclave is then closed and

purged with oxygen three times. After that the pressure is set up and the valves of the reactor closed. The temperature and stirring are set up to desired values.

The reactions are carried out for desired time and then the temperature is decreased with an external air cooler.

At the end, the reactant mixture is taken away and filtrated with a disposable filter (0.20µm porous length) using adequate syringe. One mL is taken for the HPLC analysis and the rest of the final solution is stored for the further analysis.

Both the t_0 and the t_{end} solutions are diluted 5 times with water before the HPLC analysis.

6.3 Analytical instruments for the reactivity tests

6.3.1 HPLC

High Performance Liquid Chromatography (HPLC) was developed in the late 1960s and early 1970s. Today it is widely applied for separations and purifications in a variety of areas including pharmaceuticals, biotechnology, environmental, polymer and food industries. HPLC has over the past decade become the method of choice for the analysis of a wide variety of compounds. Its main advantage over GC is that the analytes do not have to be volatile, so macromolecules are suitable for HPLC analysis. HPLC is accomplished by injection of a small amount of liquid sample into a moving stream of liquid (called the mobile phase) that passes through a column packed with particles of stationary phase. Separation of a mixture into its components depends on different degrees of retention of each component in the column. The extent to which a component is retained in the column is determined by its partitioning between the liquid mobile phase and the stationary phase. In HPLC this partitioning is affected by the relative solute/stationary phase and solute/mobile phase interactions. Thus, unlike GC, changes in mobile phase composition can have an enormous impact on the separation. Since the compounds have different 49 mobilities, they exit the column at different time. The retention time is the time between injection and detection. There are numerous detectors, which can be used, in

liquid chromatography such as UV, RI and MS. Detector is a device that senses the presence of the different components from the liquid mobile phase and converts that information to an electrical signal. It is important to remember that any changes in operating conditions will affect the retention time, which will affect the accuracy of identification. Quantitative analysis is often accomplished with HPLC. An automatic injector providing reproducible injection volumes is extremely beneficial, and are standard on modern commercial systems. The HPLC apparatus consists of a mobile phase reservoir, which is just a clean solvent jug, a solvent delivery system consisting of a pump for delivering precise, reproducible and constant amount of mobile phase, a sample inlet, the column, a detector with associated electronics, and some kind of interface to the outside world such as a computer. The pump, which is used to deliver the mobile phase solvent at a uniform rate often operates at pressures ranging from 500 - 5000 p.s.i. These high pressures are needed because the stationary phase column packing consists of very small, tightly packed particles. High pressure should be applied to push the mobile phase through this stationary phase at a reasonable flow rate. HPLC is just one type of liquid chromatography, meaning the mobile phase is a liquid. Reversed phase HPLC is the most common type of HPLC. What reversed phase means is that the mobile phase is relatively polar, and the stationary phase is relatively non-polar. Thus non-polar compounds will be more retained (i.e. have longer retention times) than a polar compound. In normal phase HPLC, the mobile phase is relatively non-polar and the stationary phase is relatively polar. Other more general types of HPLC include partition, adsorption, ion-exchange, size-exclusion, and thin-layer chromatography. The products obtained were analyzed using an HPLC Shimadzu equipped with a Synergi column. The characteristics of the column are:

P/No.: 00D-4387-B0

Desc. : Synergi 2.5u Hydro-RP 100A

Size: New Column 100 x 2.0mm

S/No.: 684470-2

No.:5380-12

The identification of the products was done comparing the HPLC chromatograms to the standards as presented below:

Furfural: Retention time of 7 min (conditions of analysis described above)

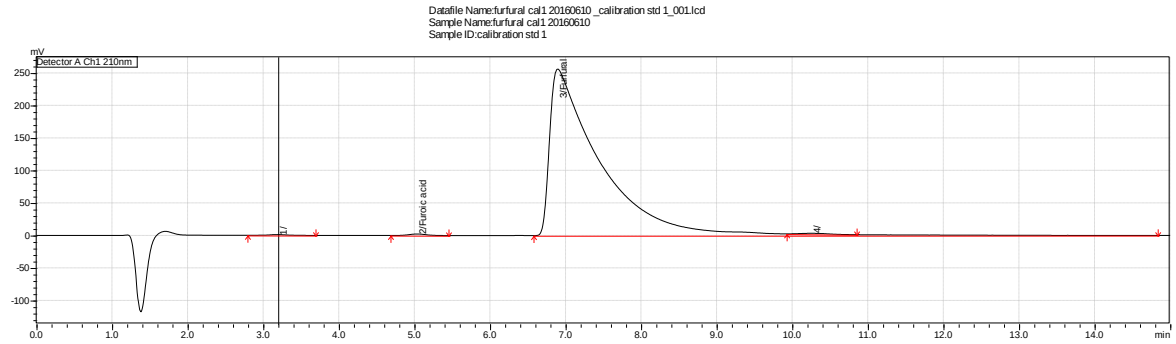

Furoic acid: Retention time of 5 min (conditions of analysis described above)

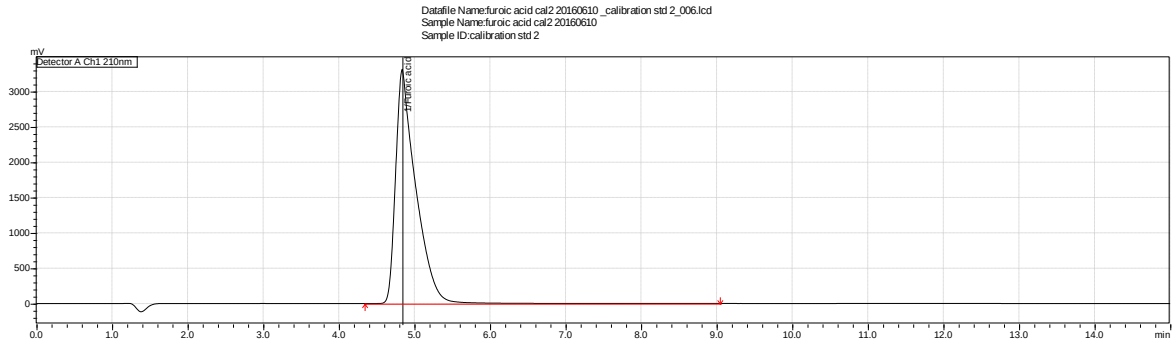

5-methyl furfural: Retention time of 18 min (conditions of analysis described above)

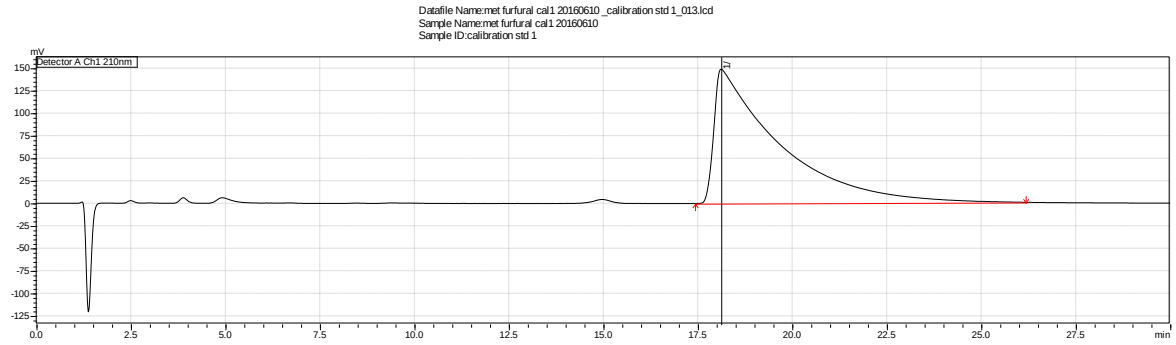

5-methyl furoic acid: Retention time of 14 min (conditions of analysis described above)

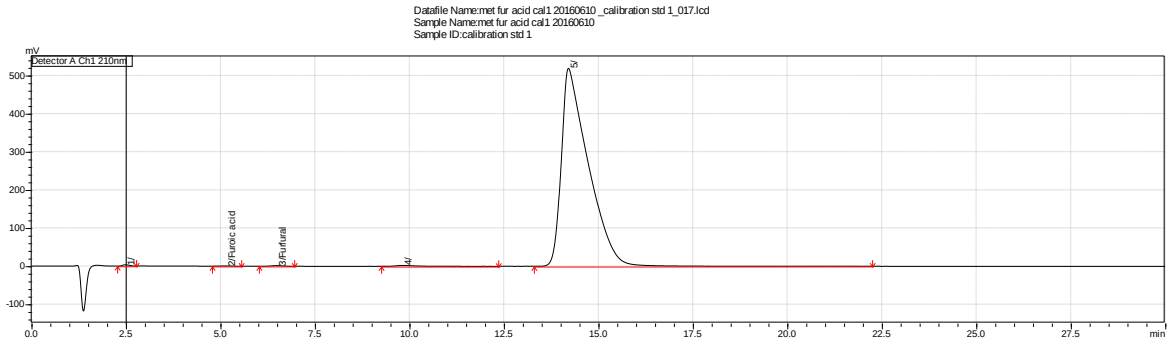

HPLC calibration

The conditions of the analysis: Flow 0,300mL/min, 0,005 mol H_2SO_4, T=40°C and a Pmax of 230 bar. The time of analysis was 15 min for furfural analysis and 60 min in case of 5-methyl furfural analysis.

- **Furfural calibration:**

Concentration [mol/L]	Area HPLC
0,003007	9479013
0,005011	14636358
0,007016	21694024
0,010023	32082002
0,015034	45071198

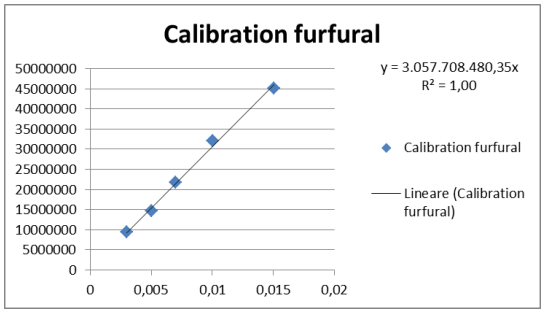

- **Furoic acid calibration:**

Concentration [mol/L]	Area HPLC
0,0029946	24845856
0,0049909	38856415
0,0069873	55584497
0,0099819	78157625
0,0149728	119560143

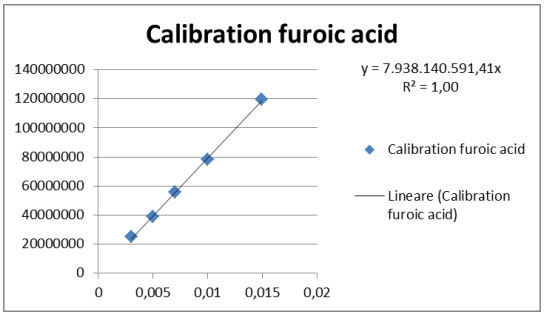

- **Maleic acid calibration:**

Concentration [mol/L]	Area HPLC
0,003014	6520568
0,005024	11381266
0,007033	15942730
0,010047	22256782
0,015071	32526515

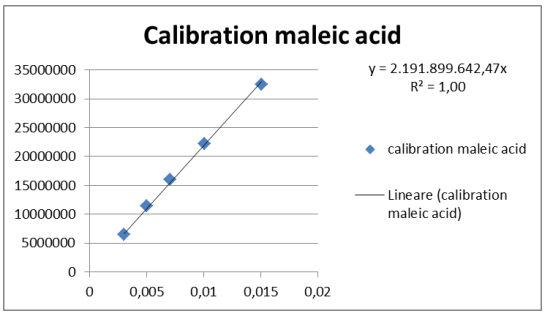

- **5-methyl furfural calibration**

Concentration [mol/L]	Area HPLC
0,002992	17558525
0,004986	28741821
0,006981	40656757
0,009973	57598043
0,014959	87704457

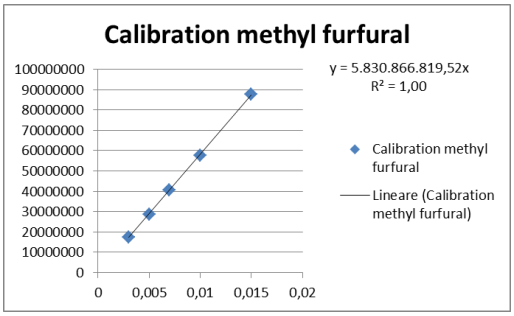

- **5-methyl furoic acid calibration**

Concentration [mol/L]	Area HPLC
0,0030053	104208424
0,0050088	157333733
0,0070124	221917363
0,0100177	292344739
0,0150265	421120655

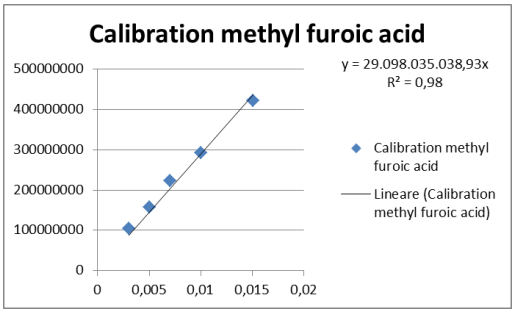

6.3.2 HPLC-MS:

High performance liquid chromatography mass spectrometry is an instrumental technique, comprising of high-pressure liquid column (HPLC) coupled to a mass spectrometer (MS), by which complex mixtures of chemicals may be separated, identified and quantified. Liquid chromatography–mass spectrometry (LC-MS, or alternatively HPLC-MS) is an analytical chemistry technique that combines the physical separation capabilities of HPLC with MS analysis. Preparative LC-MS systems can be used for rapid mass-directed purification of specific substances from such mixtures that are important in basic research, and pharmaceutical, agrochemical, food, and other industries. It allows analysis and detection even of tiny amounts of a substance. The sample flows through the column and the compounds comprising the mixture of interest are separated by virtue of their relative interaction with the column (stationary phase) and the eluent liquid (mobile phase). The latter part of the column passes through a heated transfer line and ends at the entrance to ion source where compounds eluting from the column are converted to ions. Two potential methods exist for ion production. The most frequently used method is electron ionization (EI) and the occasionally used alternative is chemical ionization (CI). For EI a beam of electrons ionize the sample molecules resulting in the loss of one electron. A molecule with one electron missing is called the molecular ion and is represented by M+. (a radical cation). When the resulting peak from this ion is seen in a mass spectrum, it gives the molecular weight of the compound. Due to the large amount of energy imparted to the molecular ion it usually fragments producing further smaller ions with characteristic relative abundances that provide a 'fingerprint' for that molecular structure. This information may be then used to identify compounds of interest and help elucidate the structure of unknown components of mixtures. CI begins with the ionization of methane (or another suitable gas), creating a radical which in turn will ionize the sample molecule to produce $[M+H]^+$ molecular ions. CI is a less energetic way of ionizing a molecule hence less fragmentation occurs with CI than with EI, hence CI yields less information about the detailed structure of the

molecule, but does yield the molecular ion; sometimes the molecular ion cannot be detected using EI, hence the two methods complement one another. Once ionized a small positive is used to repel the ions out of the ionization chamber. The next component is a mass analyzer (filter), which separates the positively charged ions according to various mass related properties depending upon the analyzer used. Several types of analyzer exist: quadrupoles, ion traps, magnetic sector, time-of-flight, radio frequency, cyclotron resonance and focusing to name a few. The most common are 66 quadrupoles and ion traps. After the ions are separated they enter a detector the output from which is amplified to boost the signal. The detector sends information to a computer that records all of the data produced, converts the electrical impulses into visual displays and hard copy displays. In addition, the computer also controls the operation of the mass spectrometer [38].

6.4 Catalyst characterization

6.4.1 XRD

In X-ray diffraction a crystalline structure, radiated with electromagnetic waves, generates the diffraction phenomenon. The principle behind this event is known as Bragg law.

$$n\lambda = 2d\,sin\theta$$

In which, considering a crystal lattice with ordered atoms:

1. n is an integer positive that indicate the order of the diffraction;
2. λ is the wavelength of the incident radiation;
3. d is the distance between two adjacent planes that compose the sample;
4. θ is the angle sized between the incident ray and the plane where the analyzed material is located.

When the Bragg law is verified the constructive interaction between the diffracted electromagnetic waves is observed. Is also possible to analyze the powders because, if they are finely blended, their orientation will be casual in the space, so

probabilistically speaking, a part of them will be able to diffract the light according to the Bragg equation.

For this reason XRD is one of the most successful analytical instrument to analyze heterogeneous catalysts. The strengths of this method are in the very small amount of sample needed and the simplicity of sample preparation. X-ray diffraction has been applied to many different types of applications including thin film analysis, sample texture evaluation, monitoring of crystalline phase and structure, and investigation of sample stress and strain [39]. Furthermore, the substance remains unchanged after the process of analysis, giving the possibility to recover it.

The resulting diffractogram have on the y axe the intensity of the scattering signal and on the x axe an angular value in 2θ, that's because source and the detector move simultaneously.

Every angle is characteristic of a diffraction of the incident light from structures with different d, which can be traced back.

The intensity parameter depends on the chemical nature and the distribution of the atoms in the phase. Crossing the data from the position and the intensity of the signals is then possible to get a complete screening of the catalyst.

With XRD techniques is possible to define:

1. the crystallinity of a sample;
2. an evaluation of the microcrystals dimension;
3. the type of phase;
4. the dimension of the unit cell and the types of atoms which compose it

Following the aim to calculate the microcrystal dimension is possible to use the Scherrer equation.

$$L = \lambda * K / (\beta * cos\theta)$$

In Which:

1. L is the evaluation of the crystal dimension along the perpendicular to the reflection plane;
2. λ represents the wavelength of the incident radiation;

3. K is a constant (can be approximated to 0,9-1);
4. β is the full width at half maximum of the peak (FWHM);
5. θ is the angle sized between the incident ray and the plane where the analyzed material is located.

Powder Xray diffraction (XRD) patterns were recorded on a Bruker D8-Advance X-ray powder diffractometer operated at an accelerating voltage of 40 kV and an emission current of 40 mA with Cu Kα radiation. Samples were scanned over the range of 10° - 70°, step size of 0.014° and a time of 19,2 s par step. The setting of 10 mm divergence, fent primaire Soller 2,5° were used.

6.4.2 XRF

X-ray fluorescence is a powerful quantitative and qualitative analytical tool for elemental analysis of materials. It is ideally suited to the measurement of film thickness and composition, determination of elemental concentration by weight of solids and solutions, and identification of specific and trace elements in complex sample matrices. XRF analysis is used extensively in many industries including semiconductors, telecommunications, microelectronics, metal finishing and refining, food, pharmaceuticals, cosmetics, agriculture, plastics, rubbers, textiles, fuels, chemicals, and environmental analysis. The method is fast, accurate, non-destructive, and usually requires only minimal sample preparation. When elements in a sample are exposed to a source of high intensity X-rays, fluorescent X-rays will be emitted from the sample at energy levels unique to those elements. The basic concept for all XRF spectrometers is a source, a sample, and a detection system. The source irradiates the sample and a detector measures the fluorescence radiation emitted from the sample. In most cases for XRF, the source is an X-ray tube. Alternatives are a radioactive source or a synchrotron. There are two main types of XRF instruments: Energy Dispersive X-ray fluorescence (EDXRF) and Wavelength Dispersive X-ray Fluorescence (WDXRF). X-ray optics can be used to enhance both types of XRF instrumentation. For conventional XRF instrumentation, typical focal spot sizes at the

sample surface range in diameter from several hundred micrometers up to several millimeters. Polycapillary focusing optics collect X-rays from the divergent X-ray source and direct them to a small focused beam at 60 the sample surface with diameters as small as tens of micrometers. The resulting increased intensity, delivered to the sample in a small focal spot, allows for enhanced spatial resolution for small feature analysis and enhanced performance for measurement of trace elements for Micro X-ray Fluorescence applications. Doubly curved crystal optics direct an intense micron-sized monochromatic X-ray beam to the sample surface for enhanced elemental analysis [40]. Elemental concentration of analyses in the catalysts was determined using an energy dispersive micro-XRay Fluorescence spectrometer M4 TORNADO (Bruker). This instrument is equipped with 2 anodes a Rhodium X-ray tube 50 kV/600 µA (30 W) and a Tungsten X-Ray tube 50 kV/700 µA (35 W). For sample characterization, the X-rays Rhodium with a polycapillary lens enabling excitation of an area of 200 µm was used. The detector used was a Silicon-Drift-Detector Si(Li) with <145 eV resolution at 100000 cps (Mn Kα) and cooled with a Peltier cooling (253°K). The elements, that can be measured by this instrument unit range from sodium (Na) to uranium (U). Quantitative analysis was done using fundamental parameter (FP) (standardless). The measurement was done under vacuum (20 mbar). A few mg of dried and ground samples were placed in a multi-well plate of thickness of 2mm for each well. Several points were measured for each sample in order to cover the sample surface with a spot size of 200 µm for each point.

6.4.3 SEM

The scanning electron microscope (SEM) uses a focused beam of high-energy electrons to generate a variety of signals at the surface of solid specimens. The signals that derive from electron-sample interactions reveal information about the sample including external morphology (texture), chemical composition, and crystalline structure and orientation of materials making up the sample. In most applications, data are collected over a selected area of the surface of the sample, and a 2-dimensional image is generated that displays spatial variations in these properties.

Areas ranging from approximately 1 cm to 5 microns in width can be imaged in a scanning mode using conventional SEM techniques (magnification ranging from 20X to approximately 30,000X, spatial resolution of 50 to 100 nm). The SEM is also capable of performing analyses of selected point locations on the sample; this approach is especially useful in qualitatively or semi-quantitatively determining chemical compositions (using EDS), crystalline structure, and crystal orientations (using EBSD). [41]

6.4.4 TEM and HRTEM

Transmission Electron Microscopy (TEM): In electron microscopy as in any field of optics the overall contrast is due to differential absorption of photons or particles (amplitude contrast) or diffraction phenomena (phase contrast). The method provides identification of phases and structural information on crystals, direct images of surfaces and elemental composition and distribution. Modes of operation and mechanisms of contrast and of imaging are essentially the same as in TEM but the main advantage of HRTEM is the ability to carry out microanalysis at very high resolution (Energy Dispersive X-ray Spectroscopy and X-mapping analysis). Energy dispersive X-ray spectroscopy (EDS) is the analysis of characteristic X- rays provides identification and quantification of elements with $Z > 10$; improvements in X-ray detectors should reduce this limit to $Z=6$.

HRTEM: A high-resolution transmission electron microscope (HRTEM, model JEOL JEM 3010) operated at 300 kV was used to investigate both the morphologic and crystalline features of the Au NPs. The samples were prepared by dispersing the catalyst powder in ethanol at room temperature and then depositing them onto a 400 mesh carbon-coated Cu grid. The histograms of the nanoparticle size distribution, assuming a spherical shape (in the case of Au) were obtained from measurements of more than 200 particles found in arbitrarily chosen regions of the grid. The histograms of the Au-based NPs were fitted considering a lognormal distribution.

6.5 *Catalysts synthesis*

6.5.1 Synthesis of Hydrotalcite:

HT material was prepared using two different molar ratios between Mg and Al (3:1 and 5:1). Known from the literature co-precipitation method was used. In more details, a solution of $Mg(NO_3)_2*6H_2O$ and $Al(NO_3)_3$ was dropped into a solution of $Na_2CO_3*10H_2O$. During the reaction, the pH was constantly controlled between 9.8 and 10.2. After that, the precipitate was filtered, dried and calcined at 450°C for 4h.

6.5.2 Addition of ZrO_2 to the HT:

ZrO_2 on the HT was prepared using a "wet impregnation" method. In more details, the zirconium butoxide was dissolved in butanol and dropped on the HT that has to be dried every time it reached the "mud point". After the impregnation the catalyst was calcined at 450°C for 4 h.

6.5.3 Gold nanoparticles supported on HT, ZrO_2/HT or VPP:

This catalyst was prepared by a chemical reduction with hydrazine. This method involves the reduction of metal salts in solution or suspension by reducing agents. Chemical reduction methods are extensively used for the metallic nanoparticles preparation because they are reproducible and easy to perform. The size and growth of the nanoparticles can be controlled by the reduction condition such as: temperature, nature of the reducing agents, and nature of the solvent.

In more details: the reaction flask was fitted with a reflux condenser and a thermocouple for the control of the reaction temperature. A suspension of the support (HT, ZrO_2/HT or VPP) (1 g in 50 mL of water) and a suspension of $HAuCl_4$ were stirred for 15 min at room temperature. Temperature was then set up to 50°C. Then 3 mL of 80 % aqueous hydrazine was added. Reaction was finished after 30 min at 50C °C and with a stirring frequency of 600 rpm. After reduction the solid was filtered, washed with distilled water and dried in the oven at 100 °C over night.

The reduction of gold with hydrazine is expected to proceed according to the following reaction:

$AuCl_4^- + N_2H_4 + 2OH^- \rightarrow Au^0 + N_2 + 4Cl^- + 2H_3O^+$

The reagents used for this synthesis were of commercial grade: gold(III) chloride trihydrate was purchased from Sigma Aldrich (≥49.0% Au basis). Hydrazine hydrate solution [$N_2H_4*H_2O$] – 78-82 % water solution was purchased from FLUKA (pure for analysis).

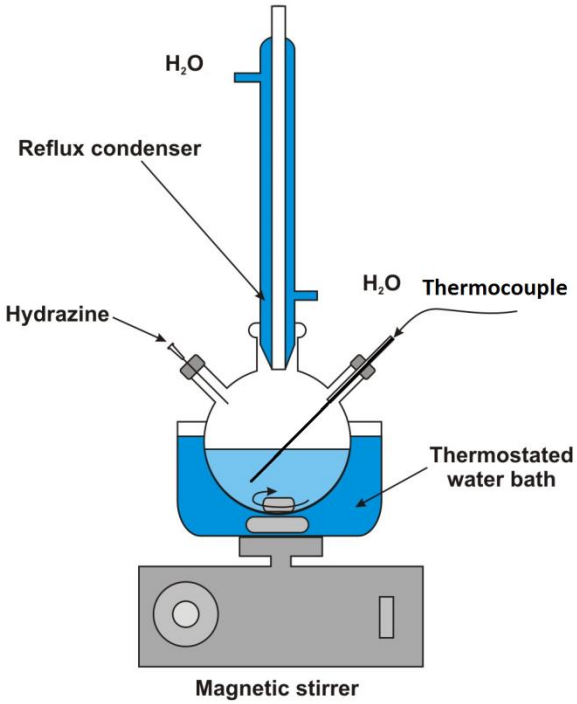

Figure 11. *Instrumental setting for the Au reduction-precipitation method*

After the tests using gold supported catalysts another type of catalyst has been tested. VPP, industrial Du Pont material is generally very active catalyst often used in the gas phase oxidation of butane to maleic anhydride (a very interesting product that can be, theoretically furfural).

6.5.4 VPP industrial synthesis:

The best-suited catalyst known for the selective oxidation of n-butane to MA is vanadyl pyrophosphate $(VO)_2P_2O_7$ (VPP), a bulk vanadium-phosphorus mixed oxide with a particular crystalline structure. In the scientific literature many different

preparation methods are reported, however there is a general agreement on these following common steps [42]:

a) synthesis of the catalyst precursor: vanadyl hydrogenphosphate hydrated, $VOHPO_4 \cdot 0.5H_2O$ (VPO); in the synthesis, the most common reactants used are vanadium pentoxide V_2O_5 as a source of V^{5+} and phosphoric acid H_3PO_4 as a source of P^{5+}.

b) thermal treatment (calcination) of the precursor to generate the active phase $(VO)_2P_2O_7$ (VPP);

c) activation of the catalyst vanadyl pyrophosphate.

The precursor (VPO) was prepared on a commercial scale in an organic medium with *iso*-butanol and benzyl alcohol. This was followed by micronization to 1 -2 µm, then spraydried with polysilicic acid to form a porous silica shell; containing up to 10% silica. The catalyst precursor ($VOHPO_4 \cdot 0.5H_2O$) was then calcined at 390°C in the generator zone of the reactor, to form the active phase catalyst $(VO)_2P_2O_7$ [43].

RESULTS and DISCUSSION

This chapter of the thesis is composed of two main parts. The first one concerns the synthesis of the catalysts and their characterization. The second presents the catalytic tests that were performed. The main goal of the second part is firstly to test all catalytic systems prepared and, secondly, trying to optimize reaction condition, which would permit to obtain the best catalytic performances.

7 Screening of the catalysts

Several catalytic systems have been synthetized and tested in order to find the best catalyst for the synthesis of furoic acid, 5-methyl furoic acid and maleic acid. The catalysts used in our work are listed below. In the case of homemade catalysts the preparation method is also described in details. Various catalysts based on hydrotalcite were tested. In particular:

- Hydrotalcite (HT) with a 3:1 wt.% ratio between Mg and Al
- HT 5:1
- 2wt.% Au on HT 3:1
- 2wt.% Au on HT 5:1
- 2,5wt.% ZrO_2 on HT 3:1 (ZrO_2/HT mixed oxide)
- 2% Au on ZrO_2-HT 3:1

7.1 Catalysts characterization

XRD characterization was performed using D8 Diffractometer of the REALCAT platform. Also XRF and SEM were performed for most of the catalysts. The aims of this study were to check the structure of the prepared catalysts and, if possible, to estimate the average Au particle size The results are presented below:

7.1.1 HT 3:1:

The first XRD analysis has been performed on the HT support (3:1). As could be seen on Fig. 14 characteristic diffraction peaks related to the HT structure are present.

However, the presence of other phases (mixed oxides) is also evidenced. In addition, some impurity of NaCl and $NaNO_2$ was detected in both SEM and XRF (as described below). It is due to the catalyst preparation method used for the synthesis and insufficient cleaning of the solid during the filtration.

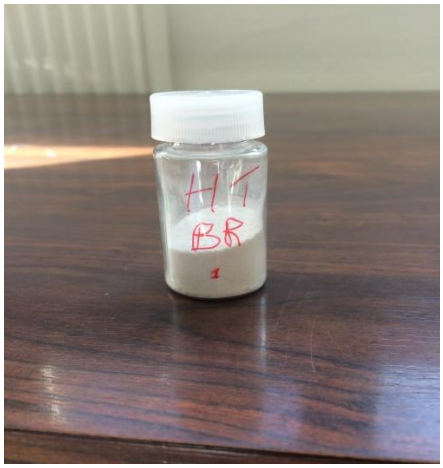

Figure 12. HT3:1

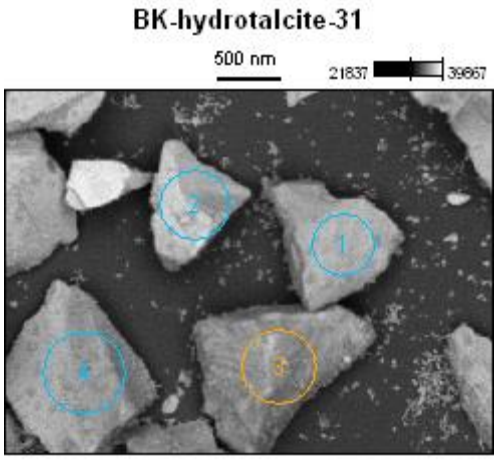

Figure 13. SEM image HT3:1

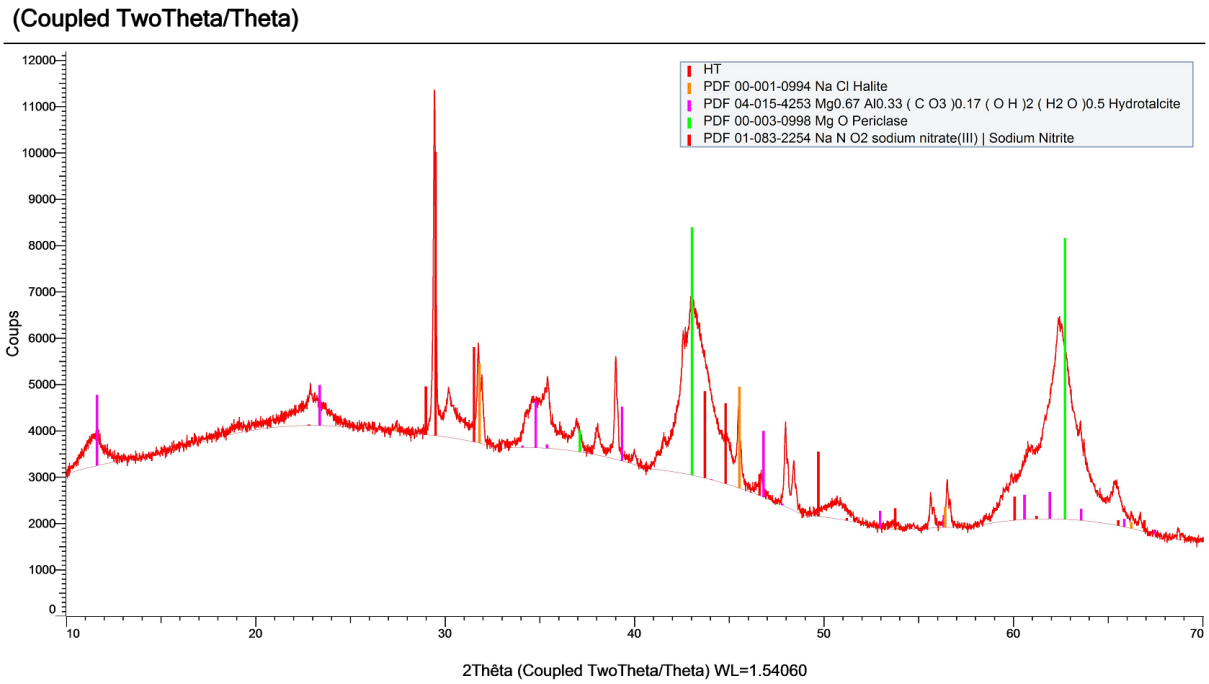

Figure 14.X ray diffraction pattern of HT 3:1 catalyst

The XRF analysis confirms the presence of Na and other small amounts of impurities due to the preparation method. The Mg/Al ratio is close to 2 but lower than 3

expected. This could be due to the XRF analysis, which does not take into account the oxygen. The real values could be confirmed only by ICP analysis.

XRF HT 3:1

	Na	Mg	Al	Ca	Fe	Ni
Mean value:	10,51	50,07	38,38	0,96	0,04	0,04
Std. Abw.:	3,77	1,27	2,70	0,30	0,05	0,05
Std. Abw. rel. [%]:	35,88	2,54	7,03	31,61	116,9	124,9
Conf. interval:	0,52	0,18	0,38	0,04	0,01	0,01

7.1.2 2% Au/(HT 3:1):

Different diffraction peaks originate from HT are present in the diffractogram of this material. However, the presence of other phases was also evidenced. Indeed, it is possible to observe peaks corresponding to the MgO and Al_2O_3 oxides and also peaks from metallic gold (at about 38 and 44°). The peaks of contaminants (NaCl and $NaNO_3$) are no more present because of the method of preparation used for gold deposition (reduction with hydrazine in water). As expected the NaCl was removed from the material during the washing steps. It was also possible to identify reflection peaks originated from gold (green lines). The average gold particle size estimated using Scherrer formula (see experimental part) is about 21 nm.

Figure 15. Au / (HT 3:1)

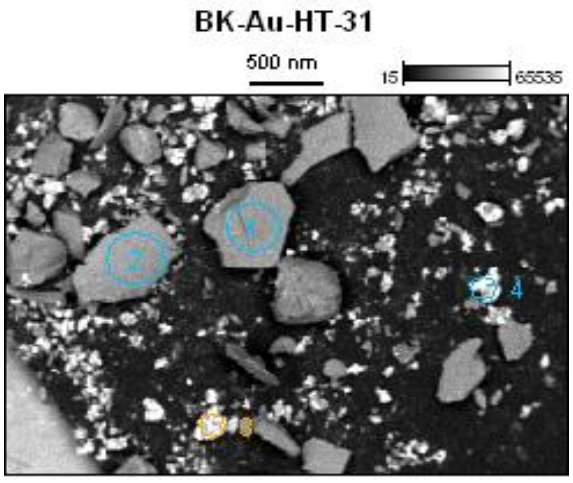

Figure 16. SEM image Au / (HT 3:1)

As appeared from the SEM results the Au is not homogenously dispersed on the surface of the catalyst. From the SEM image it is also evident that the average Au particle size is bigger than expected.

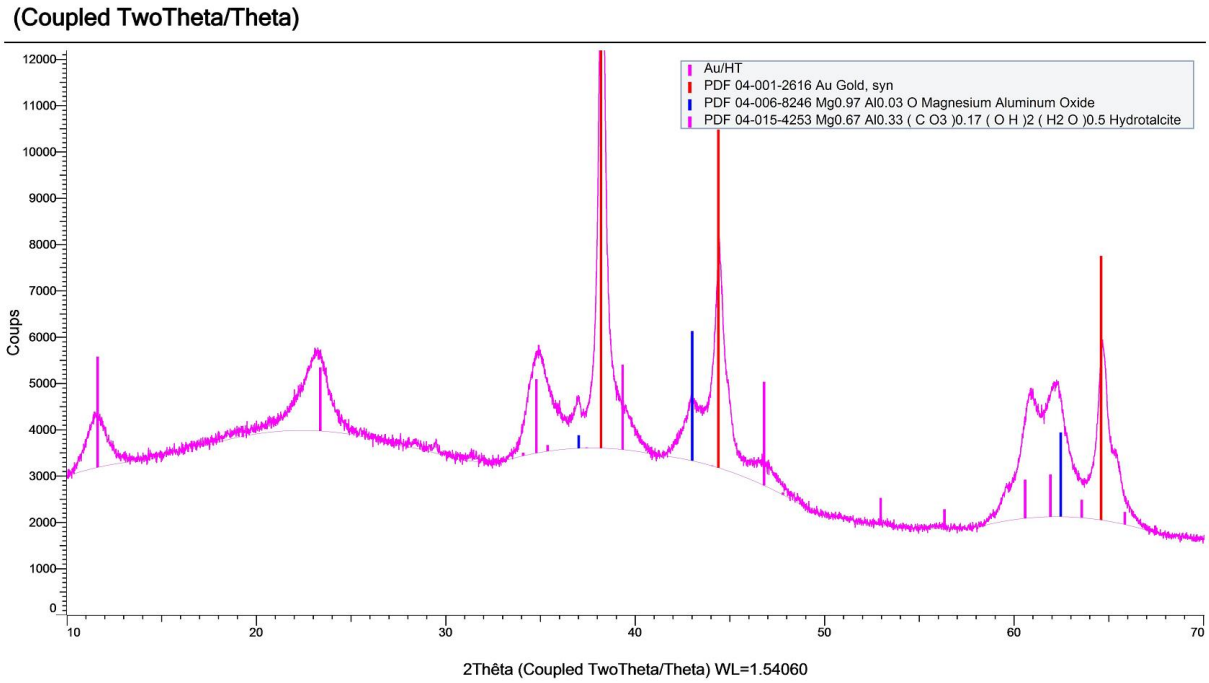

Figure 17. *X ray diffraction pattern of Au/HT3:1 catalyst*

The XRF confirmed also the presence of gold in the material. However, the values are a not exactly as expected. This could be due also to the fact that XRF is not a accurate for quantitative analysis.

XRF Au/HT3:1

	Mg	Al	Ca	Fe	Rh	Au
Mean value:	38,61	19,61	0,72	0,05	0	41,02
Std. Abw.:	0,61	0,59	0,02	0,01	0	1,18
Std. Abw. rel. [%]:	1,57	2,99	2,82	7,39	0	2,88
Conf. interval:	0,14	0,13	0,01	0,01	0	0,26

7.1.3 2% Au/HT 5:1:

This catalyst was also characterized using the same techniques. In this case the expected Mg to Al ratio is about 5. The XRD pattern of this catalyst shows lower intensity of the diffraction peaks originates from Au. This is probably due to the

sensibility of this type of catalyst preparation that can involve substantial differences with small variation.

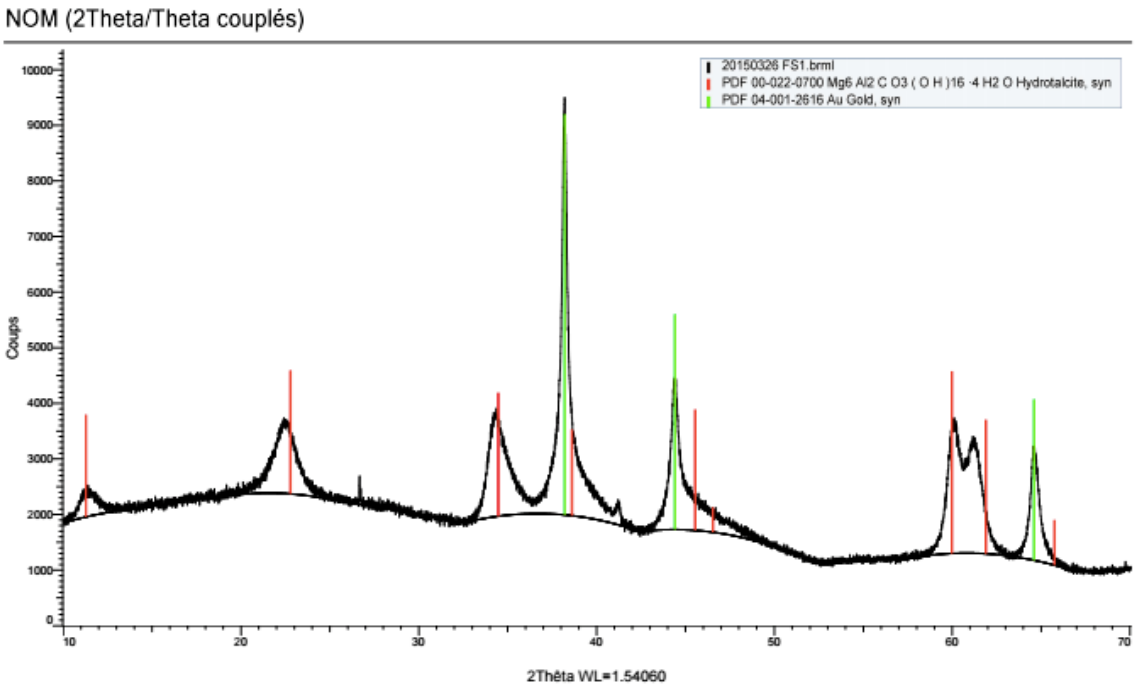

Figure 18. *X ray diffraction pattern of 2% Au/HT5:1 catalyst*

7.1.4 ZrO_2 / (HT 3:1) & Au / ZrO_2 /(HT 3:1):

Both XRD patterns are very similar to that observed in the case of HT samples. The characteristic structure of HT could be confirmed. The presence of Zr found during the SEM analysis is not confirmed by XRD. This could be due to the amorphous character of the ZrO_2.

The SEM analysis shows that the atomic ratio Mg/Zr is close to the expected (between 1-5%) values. However, the results confirmed also the presence of NaCl on the surface (problem with sample washing). The SEM analysis of the Au / ZrO_2 /(HT 3:1) confirms that the dispersion of Au is not very homogenous. Furthermore the quantity of Zr on the surface decreased as compared to free Au sample, probably because of the gold deposition.

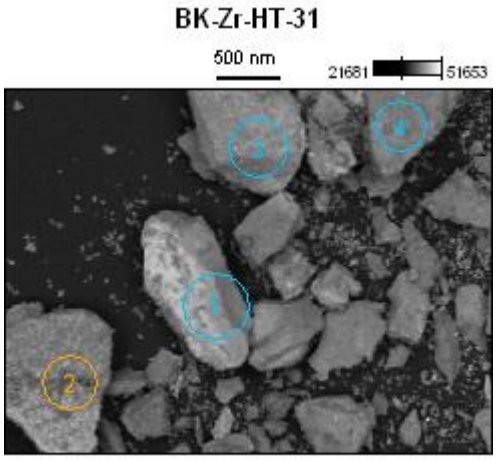

Figure 19. *SEM image ZrO_2 / (HT 3:1)*

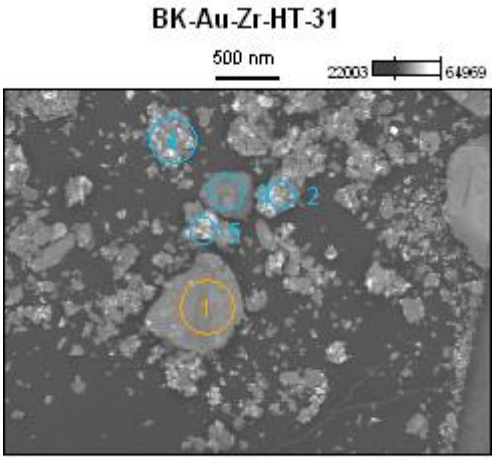

Figure 20. *SEM image Au / ZrO_2 /(HT 3:1)*

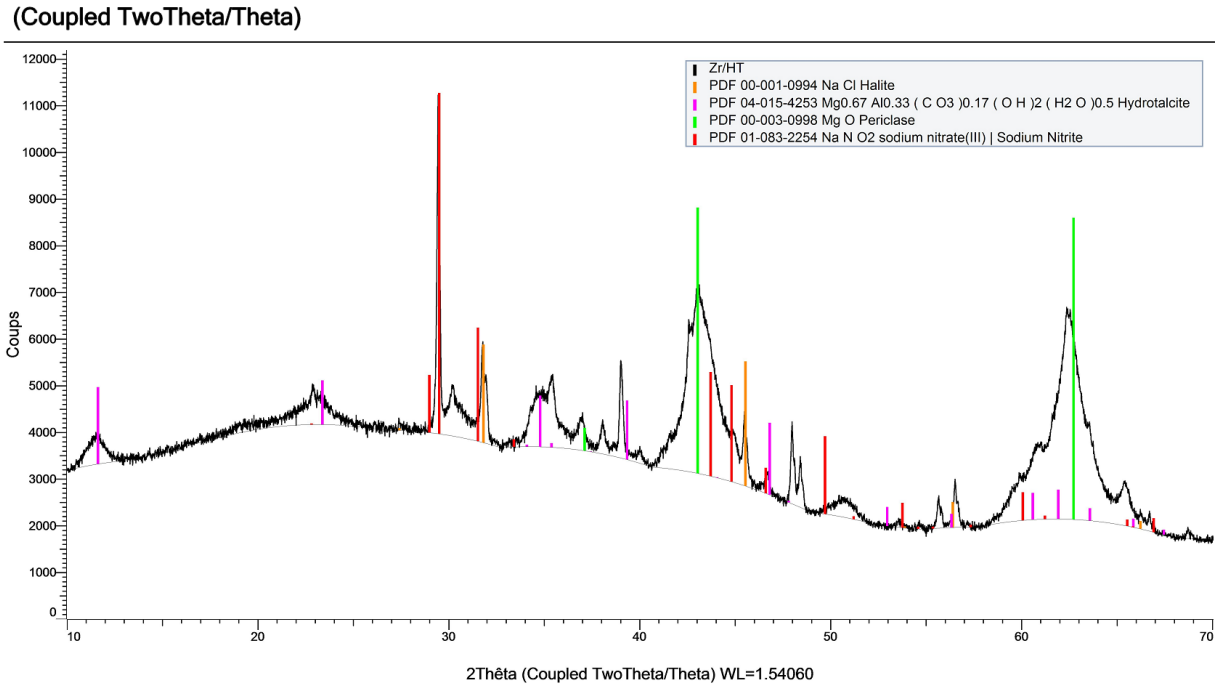

Figure 21. *X ray diffraction spectra of ZrO_2/HT3:1 catalyst*

XRF ZrO_2 / (HT3:1)

	Na	Mg	Al	Ca	Fe	Ni	Zr
Mean value:	18,92	37,50	21,19	0,80	0,15	0,01	21,22
Std. Abw.:	3,31	1,058	0,85	0,03	0,01	0,01	3,25
Std. Abw. rel. [%]:	17,47	2,82	4,03	3,18	7,66	23,14	15,30
Conf. interval:	0,58	0,18	0,15	0,01	0,00	0,001	0,57

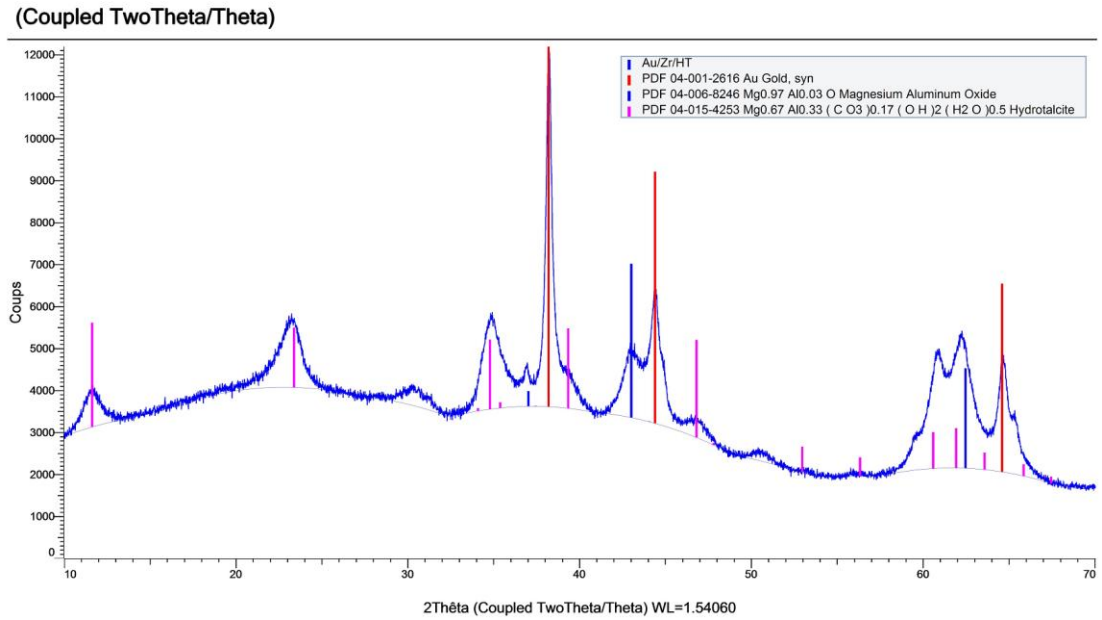

Figure 22. *X ray diffraction pattern of Au/ZrO_2/HT3:1 catalyst*

XRF Au / ZrO_2 / (HT3:1)

	Mg	Al	Ca	Fe	Rh	Au
Mean value:	49,25	33,84	1,10	0,08	0,33	15,21
Std. Abw.:	0,537	1,95	0,05	0,01	0,02	2,05
Std. Abw. rel. [%]:	1,09	5,75	4,71	10,28	5,15	13,47
Conf. interval:	0,08	0,293	0,008	0,001	0,002	0,309

7.2 ZrO_2 support analysis

To confirm the different crystalline structures of two different zirconium oxides used, a XRD analysis was performed. The XRD patterns are shown on **Figure 23** and **Figure 24**. As expected, two different crystalline structures were observed: the commercial zirconium oxide has a Baddeleyite structure (**Figure 24)**, while the "home-made" zirconium oxide is Arkelite (**Figure 23).** Moreover, XRD results confirmed also formation of large gold nanoparticles in the case of mesoporous support (Figure 23, blue lines). This could explain different catalytic activity observed in the oxidation reaction with these two samples.

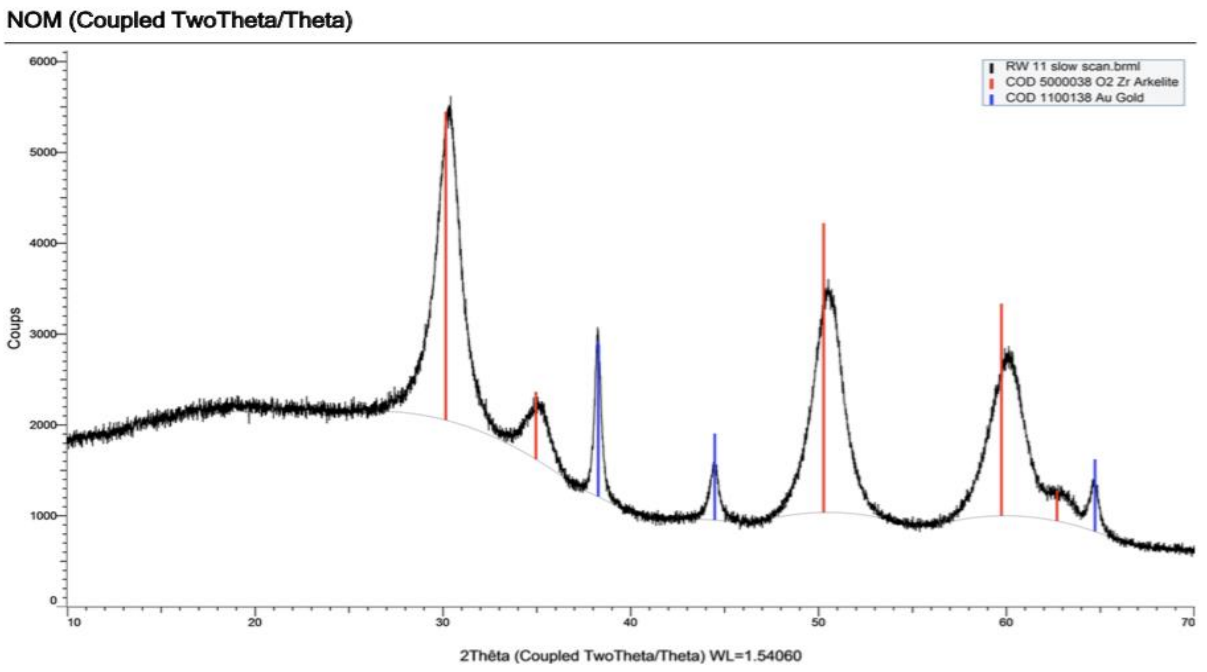

Figure 23. *X ray diffraction pattern of 3% Au/ZrO_2 catalyst prepared with mesoporous zirconium oxide*

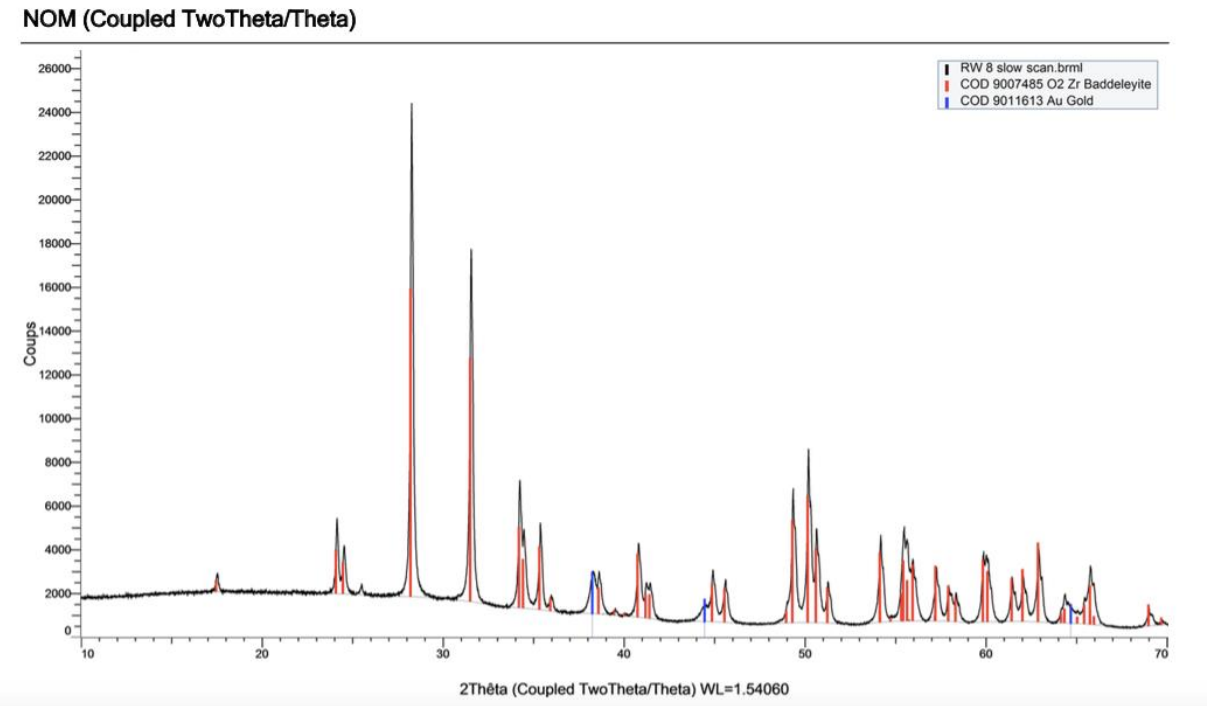

Figure 24. *X ray diffraction pattern of 3% Au/ZrO_2 sample prepared with commercial Zirconium Oxide (Sigma-Aldrich)*

7.3 VPP & Au / VPP:

On these two catalysts only the XRD and XRF analyses were performed. It is worth to note that VPP is an industrial catalyst (from DuPont) while the addition of gold nanoparticles was performed in the laboratory during the research work.

Figure 25: *VPP catalyst as received*

Figure 26: *Au/VPP catalyst as prepared*

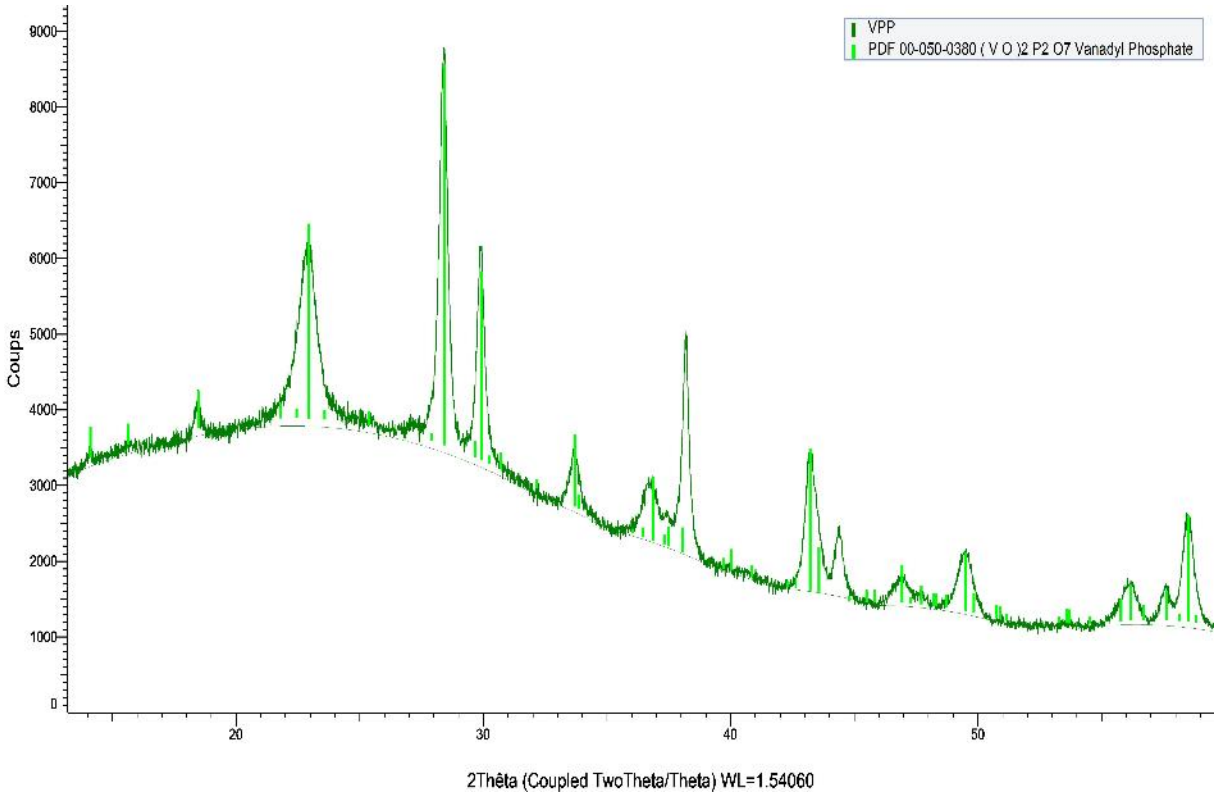

Figure 27: *X ray diffraction pattern of VPP catalyst*

The X-ray diffraction pattern of DuPont VPP sample shows characteristic peaks of the vanadyl pyrophosphate $(VO)_2P_2O_7$, confirmed its expected structure.

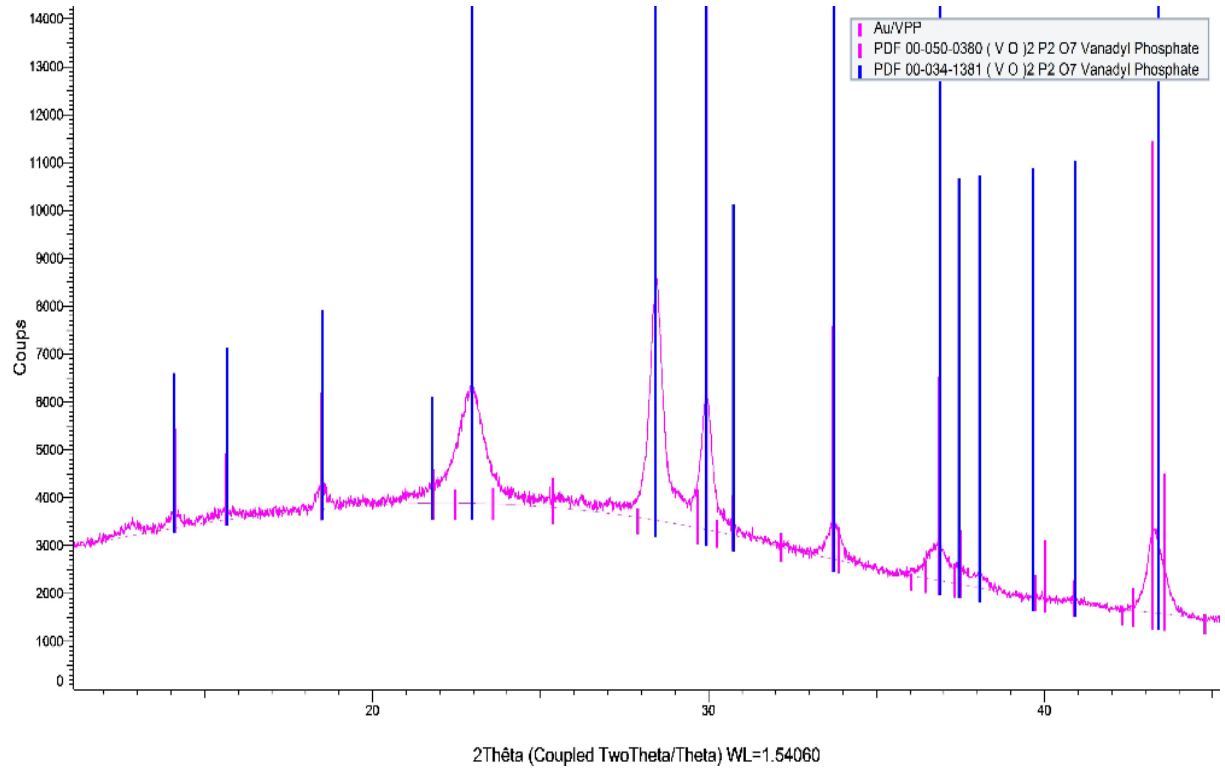

Figure 28. *X ray diffraction pattern of VPP catalyst*

The diffraction pattern of the Au/VPP sample presented in Fig. 28 shows also characteristic peaks originated from vanadyl phosphate. However, no peaks originated from gold were present even if the presence of gold was confirmed by XRF analysis. This could be explained by very small size of the gold particles (smaller than 3 nm) or by the very low Au content.

XRF VPP

	P	**V**	**Rh**
Mean value:	25,74	74,26	0
Std. Abw.:	0,22	0,22	0
Std. Abw. rel. [%]:	0,87	0,30	0
Conf. interval:	0,03	0,03	0

XRF Au/VPP

	O	V	Fe	Au	(VO)2P2O7	SiO2
Mean value:	6,67E-07	0	0,02	1,46	91,46	7,06
Std. Abw.:	8,9E-07	0	0,002	0,21	0,26	0,25
Std. Abw. rel. [%]:	133,4762	0	8,25	14,48	0,29	3,53
Conf. interval:	1,21E-07	0	0,00	0,03	0,04	0,03

The XRF analysis performed on Au/VPP confirmed that the percentage of gold deposited on bulk VPP is almost 2% (the expected value was 2% wt.), this means that the method used is suitable for the preparation of VPP supported gold nanoparticles.

The SiO_2 observed in these materials is due to the silica shell that covers the VPP particles. DuPont indicated a 10% of SiO_2.

Two catalysts (Au/HT5:1 and Au/HT3:1) were characterized using HRTEM analysis. The images are shown in Figures 29-32.

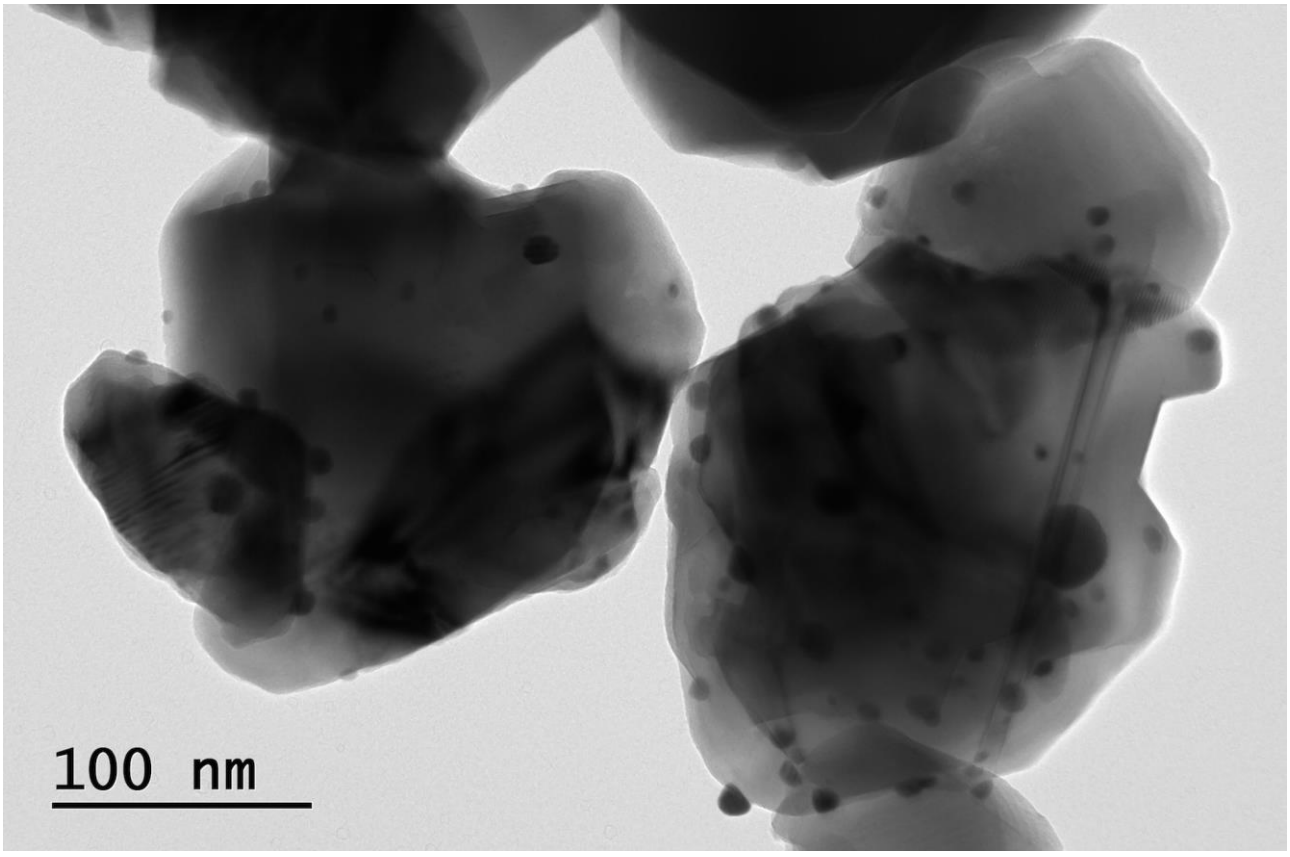

Figure 29. *HRTEM image of the Au/HT5:1 catalyst (general view)*

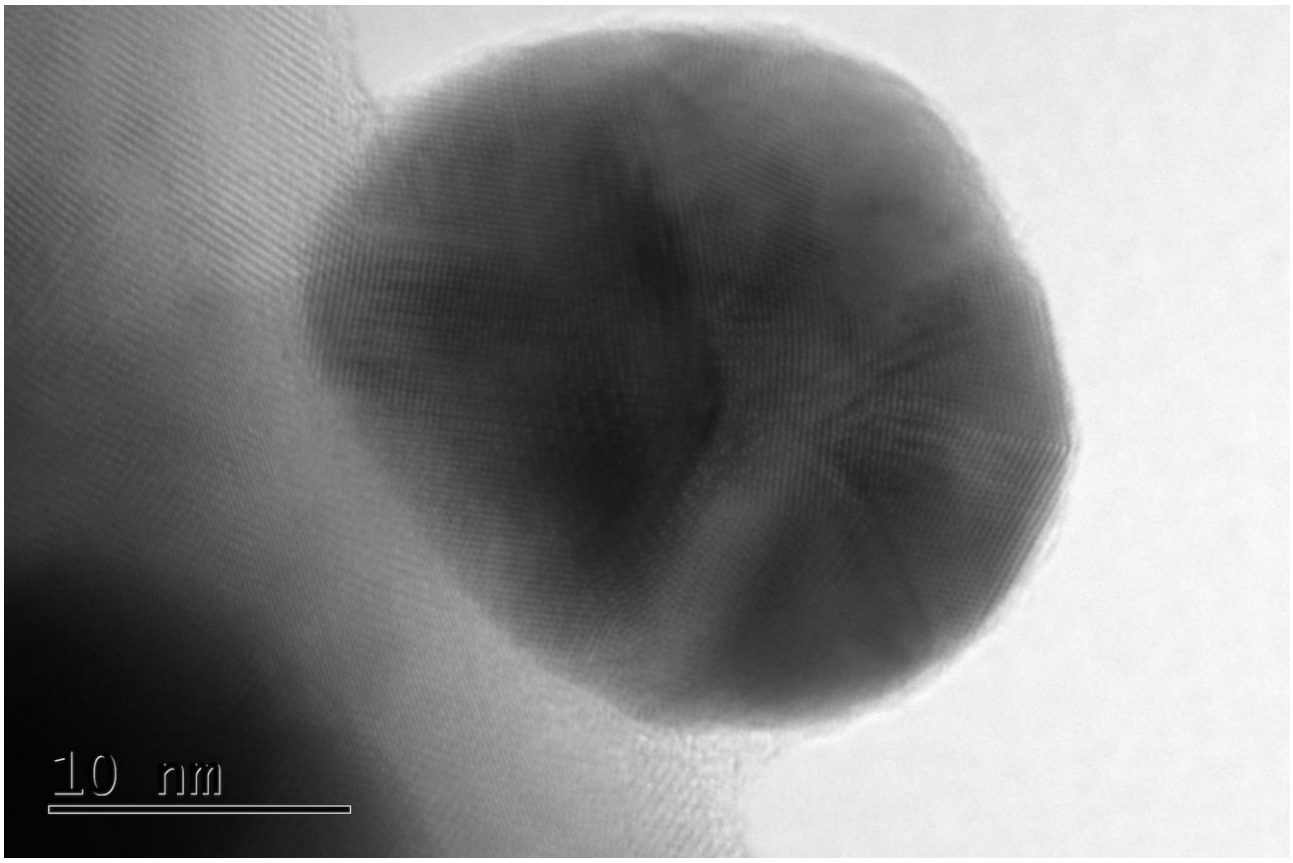

Figure 30. *HRTEM image of the Au isolated particle in Au/HT5:1 catalyst*

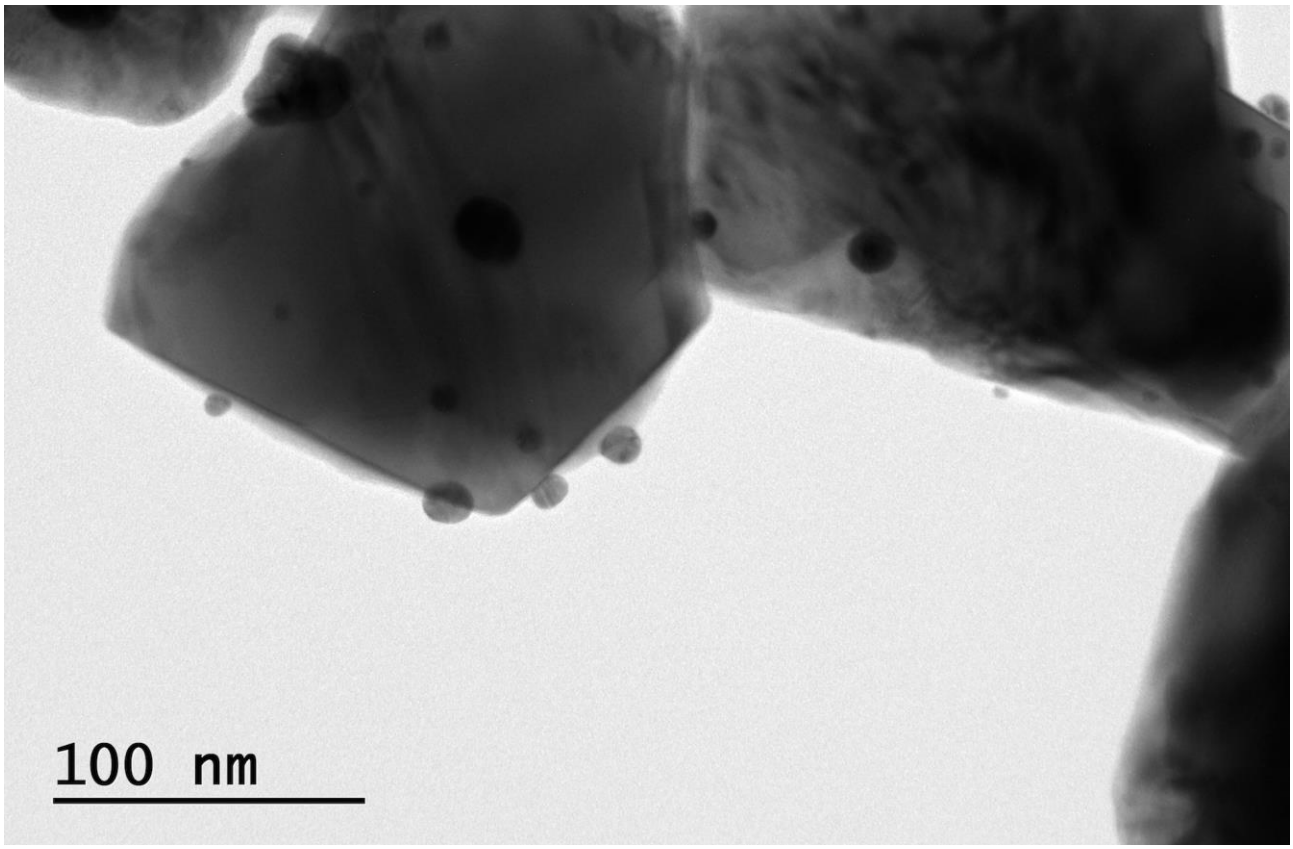

Figure 31. *HRTEM image of the Au/HT3:1 catalyst (general view)*

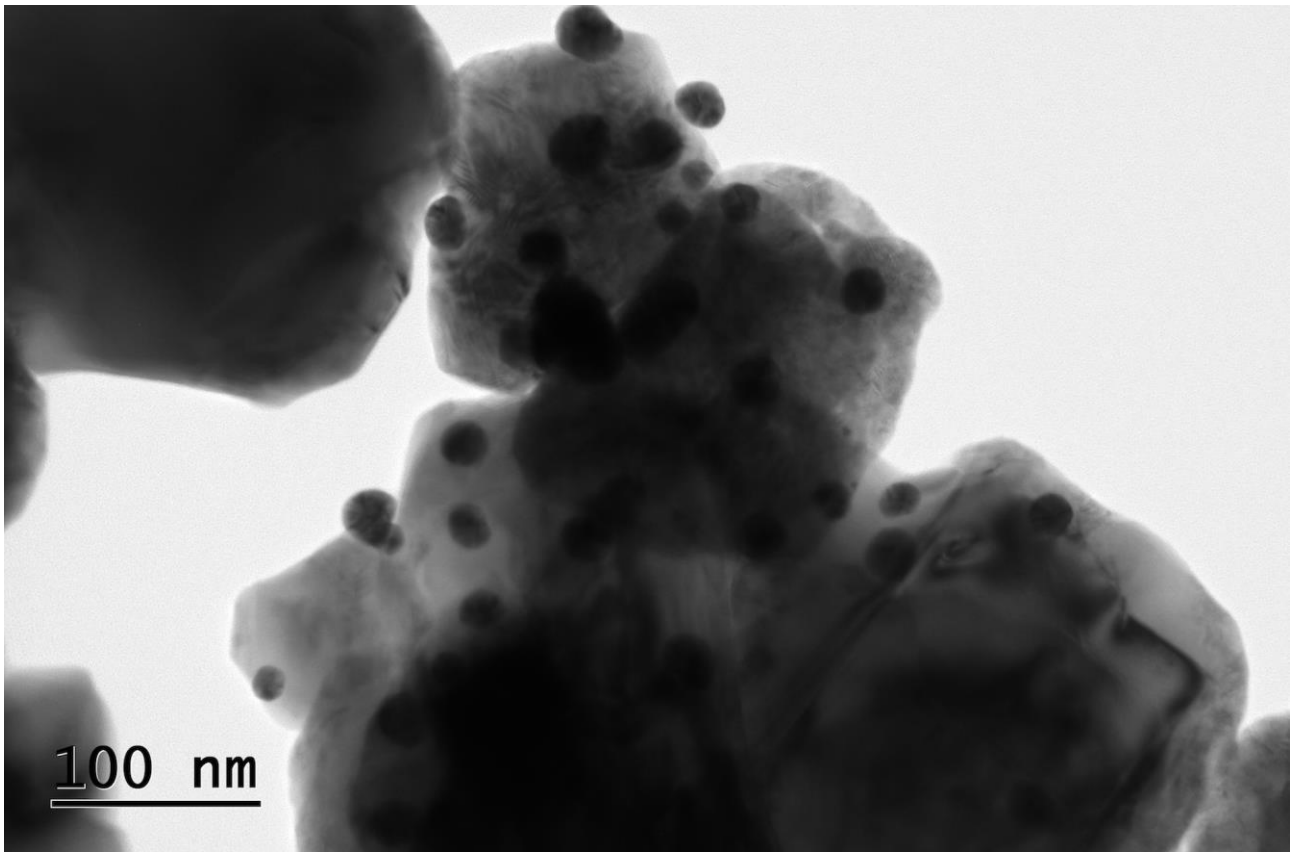

Figure 32. *HRTEM image of the Au/HT3:1 catalyst (general view)*

In case of the Au/HT5:1 catalyst (Figures 29 and 30) small particles of about 5 nm can be seen (Figure 29). However, the big Au particles of about 18 nm are also present (Figure 30). This is in good agreement with the results observed from XRD (average particle size of 20 nm). However, the most of the Au particles have size lower than 10 nm.

In the case of Au/HT3:1 catalyst (Figures 30 and 32) small gold particles are also observed but the most of them are in the particle size range 15-30 (Figure 32). This is also in good agreement with the XRD and SEM data (as described above).

7.4 Catalytic tests

During this thesis many catalytic tests on both furfural and 5-methyl furfural oxidation were made using a batch reactor. The initial purpose was the synthesis of furoic acid and 5-methyl furoic acid. Different catalysts and operating conditions were tested in order to maximize X, Y, S and carbon balance.

At the beginning of the thesis many tests using biphasic system (water+MBIK) were performed. Unfortunately, due to the problems with the analysis post-tests of the products, it was impossible to analyze them in a short time after the reaction stops. The results obtained showed high level of furfural degradation and it occurred even if the samples were stored in the fridge. This problem was evidenced by the calculation of the carbon balance on stored samples. The carbon balance was very low, indicating that unreacted furfural and products were degraded. Another problem concerned the t_0 samples. The HPLC analysis at t_0 showed a lot of irregularities, which should be probably due to the low solubility of furfural in water (non homogeneous samples). However, even if the t_0 was assumed constant for all samples the carbon balance remained still low indicating again degradation process.

In Figure 33 three results obtained using 50mg furfural, 20mL of water as solvent, 4 h as reaction time, 120°C as temperature and 6 bar of pressure and 900 rpm as stirring.

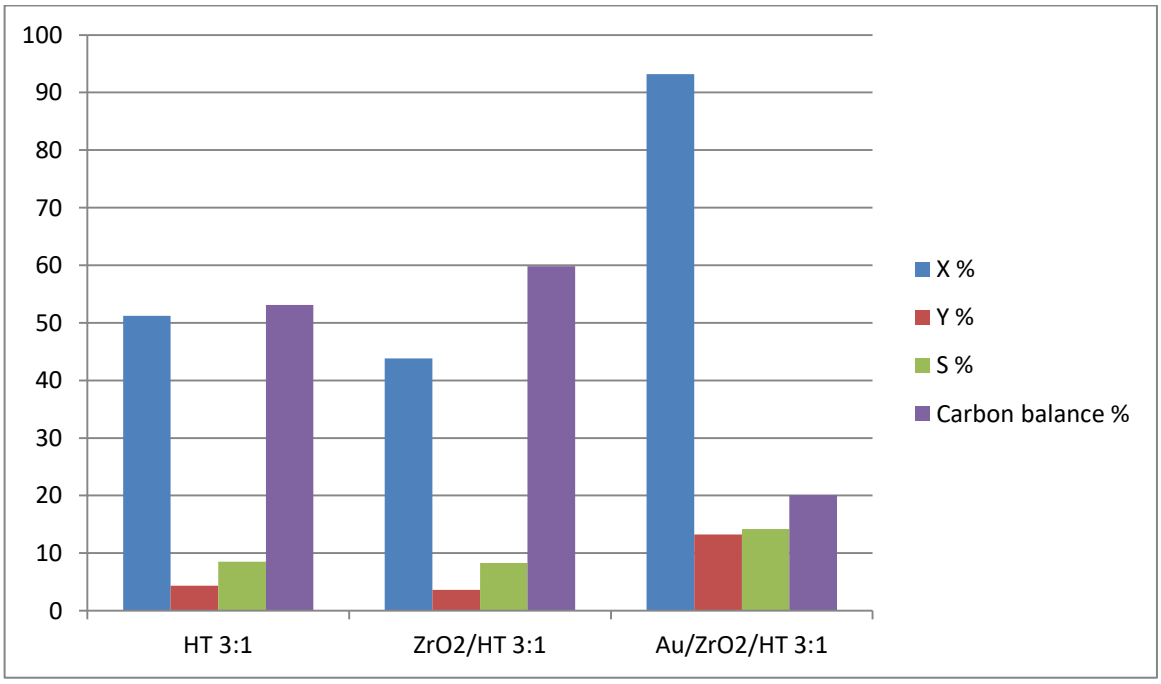

Figure 33. Comparison tests using HT, ZrO_2/HT3:1 and Au/ZrO_2/HT3:1 catalysts

Due to the problems described above new calibrations curves were performed. Moreover, new catalytic tests were performed using the same catalysts as before but with a shorter reaction time (2 h instead of 4h). The conditions are listed in Table 5.

Table 5. *Experimental conditions of the catalytic tests*

BR	reagent	V[µL]	M[mg]	P_{O2}[bar]	Catalyst	Solvent	t[h]	T[°C]
21	furfural	43	50	9	Au/HT_{51} (100mg)	H_2O (20mL)	2	110
22	methyl furfural	45	50	15	Au/HT_{51} (100mg)	H_2O+etOH (19+1)mL	2	110
23	methyl furfural	45	50	15	Au/HT_{51} (100mg)	H_2O+AcN (19+1)mL	2	110
24	furfural	43	50	15	Au/HT_{31} (100mg)	H_2O (20mL)	2	110
25	methyl furfural	45	50	15	Au/HT_{DP} (100mg)	H_2O+AcN (19+1)mL	2	110
26	methyl furfural	45	50	15	$Au/ZrO_2/HT_{31}$ (100mg)	H_2O+AcN (19+1)mL	2	110
27	methyl furfural	45	50	15	HT_{31} (100mg)	H_2O+AcN (19+1)mL	2	110
28	methyl furfural	45	50	15	Au/HT_{31} (100mg)	H_2O+AcN (19+1)mL	2	110
29	methyl furfural	45	50	15	VPP duPont (100mg)	H_2O+AcN (19+1)mL	2	110
30	methyl furfural	45	50	15	Au/VPP (100mg)	H_2O+AcN (19+1)mL	2	110
31	furfural	43	50	15	VPP (100mg)	H_2O (20mL)	2	110
32	furfural	43	50	15	Au/VPP (100mg)	H_2O (20mL)	2	110
33	furfural	43	50	15	None (100mg)	H_2O (20mL)	2	110
34	furfural	43	50	15	VPP (100mg)	H_2O (20mL)	2	90
35	furfural	43	50	15	$Au/HT_{31recycle}$ (100mg)	H_2O (20mL)	2	110

36	furfural	43	50	15	Au/HT_{31} (100mg)	H_2O (20mL)	6	110
37	methyl furfural	45	50	15	Au/HT_{51} (100mg)	H_2O+AcN (19+1)mL	6	110
38	methyl furfural	45	50	15	Au/HT_{51} (100mg)	H_2O+AcN (19+1)mL	6	130
39	methyl furfural	10	11	15	Au/HT_{51} (100mg)	H_2O+AcN (19+1)mL	2	110
40	furfural	43	50	15	Au/HT_{31} (100mg)	H_2O (20mL)	2	130
41	furfural	43	50	15	VPP (100mg)	H_2O (20mL)	2	130
42	furfural	43	50	15	VPP (100mg)	H_2O (20mL)	6	110

*BR22 and BR23 have been carried out in the same reaction conditions. The only difference is that in the BR22 experiments 1 mL of ethanol was used to solubilize methyl furfural before the test and in the case of the BR23 experiment, acetonitrile was used instead of ethanol to avoid the possibility of esterification of the acid products.

7.5 Furfural oxidation to furoic acid on Au/HT catalysts

Two different types of hydrotalcite (3:1 and 5:1, please see Experimental Part), modified with gold nanoparticles, were used. The condition in both cases were the same: 50mg furfural, 20mL of water as solvent, 2 h as reaction time, 110°C as temperature and 6 bar of pressure and 900 rpm as stirring.

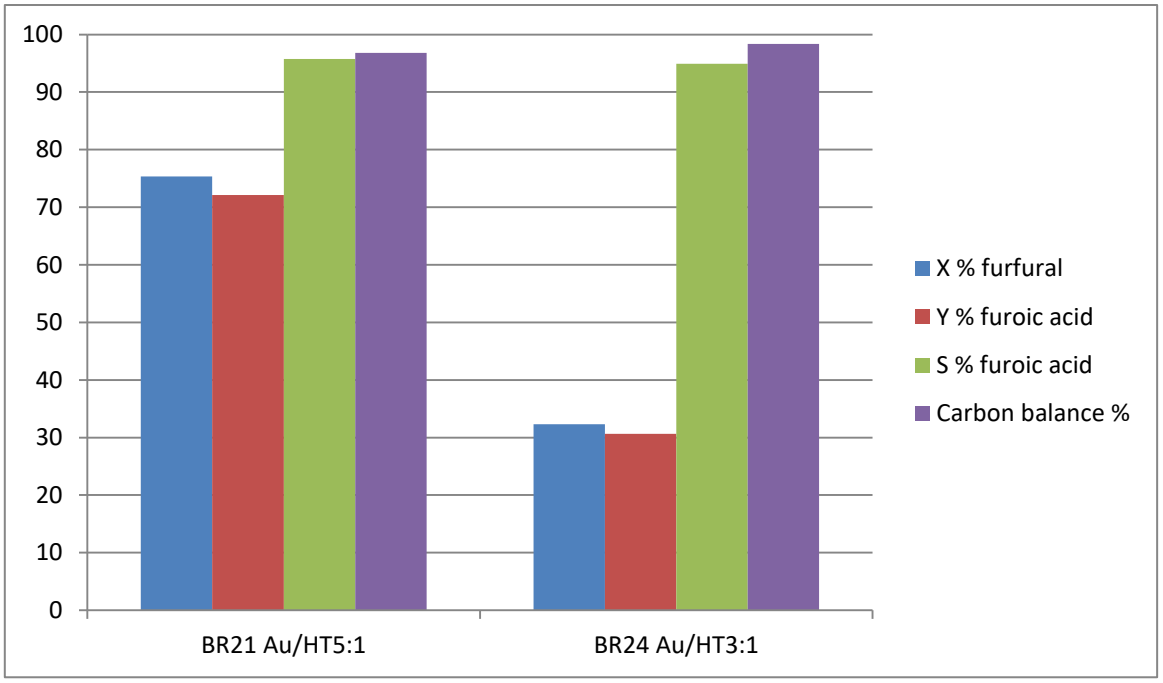

Figure 34. *Catalytic results for the Au/HT catalysts*

Both catalysts showed high selectivity to furoic acid and carbon balance was found higher than 95%. However, Au/HT5:1 catalyst shows higher conversion as compared to the Au/HT3:1 catalyst. It could be due to two factors: firstly higher ratio between Mg and Al increases the basicity of the catalyst. Higher basicity seems to improve the catalytic performances for this reaction. Secondly it is possible that in case of the HT5:1 sample smaller gold nanoparticles were obtained (as indicated by XRD studies). Smaller gold nanoparticles on 5:1 hydrotalcite can also be observed by the different colour (more light purple). However, TEM analysis is necessary to confirm this hypothesis.

7.5.1 Further investigation on catalytic oxidation of furfural

Following the interesting results from the oxidation of furfural on Au supported HT catalyst a blank test was made to confirm the catalytic activity of this catalyst. A longer time of the reaction was also tried to check the influence of the time of reaction of catalytic activity and stability of the products. For the same reasons the catalytic tests were performed at different temperatures to check the activity and stability. Catalytic results obtained are showed below.

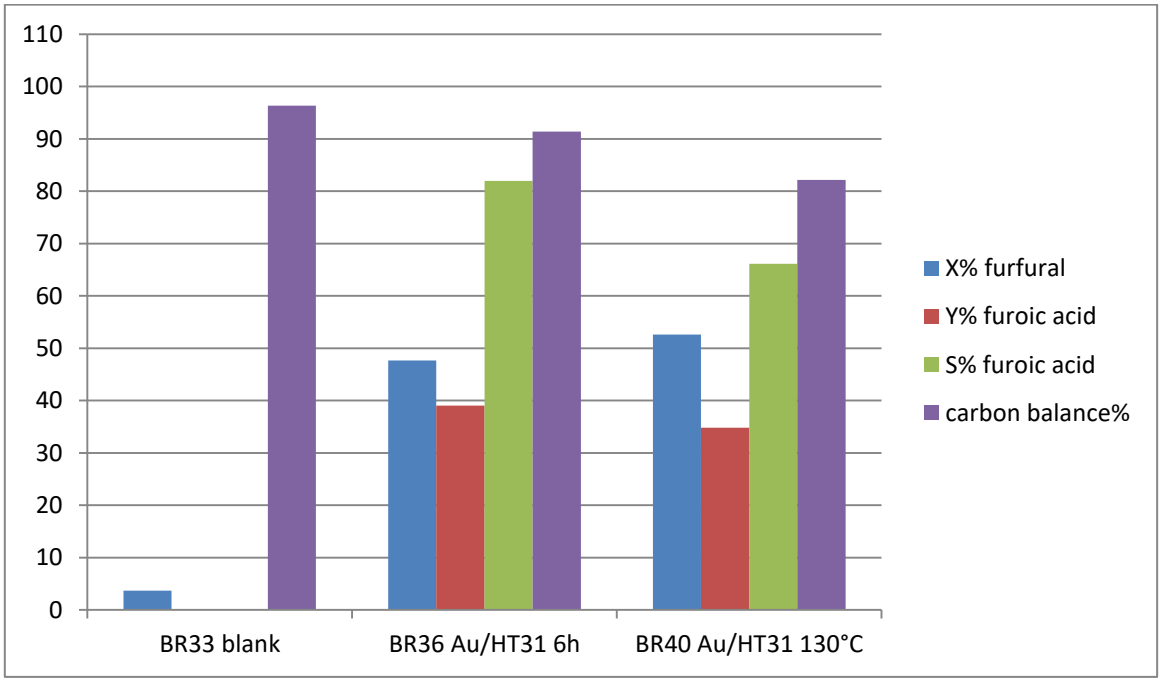

Figure 35. *Results of the furfural oxidation in different operative conditions*

BR33 corresponds to a blank test (test without catalyst). As could be seen, the degradation of furfural in the conditions of reaction (110°C, 15 bar of O2, 4 h) is not significant. As expected, formation of any product was observed.

7.5.2 Effect of the time of reaction on Au/HT activity

Table 6. Effect of the time of the reaction on catalytic activity of the Au/HT catalyst

reaction	catalyst	t[h]	X%	Y%	S%	c.b.%
BR24	Au/HT3:1	2	32,3	30,7	94,9	98,4
BR36	Au/HT3:1	6	47,6	39,0	81,9	91,4

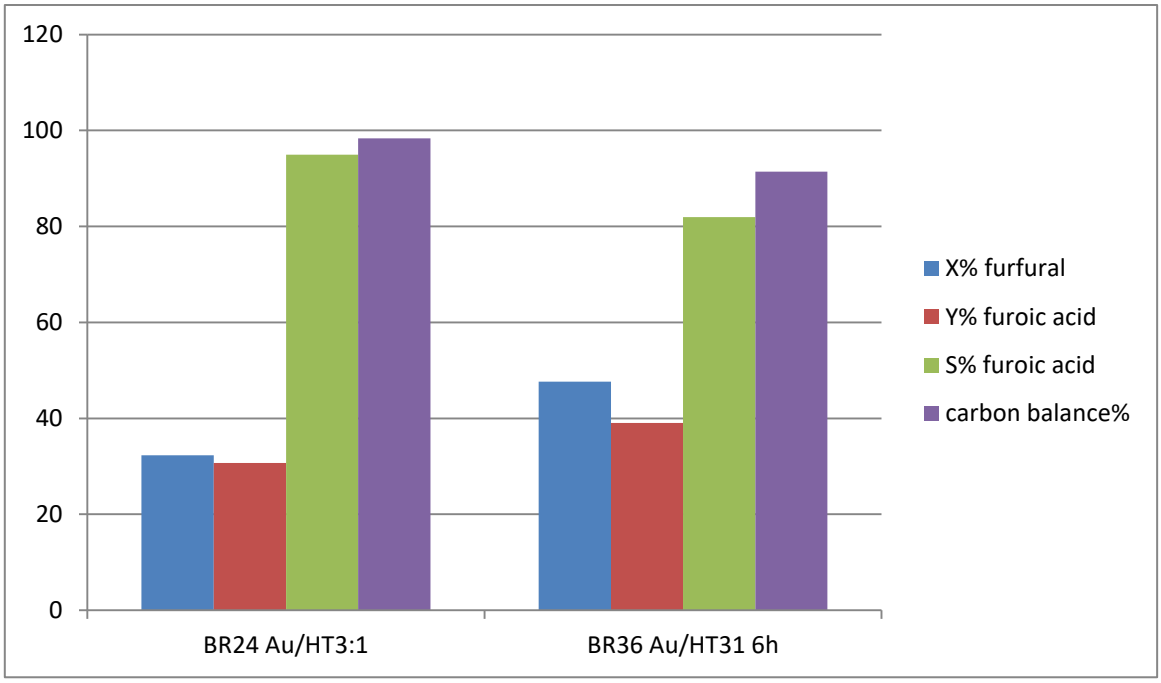

Figure 36. *Comparison between 2 different times of reaction (2 and 6 hours) with Au/HT3:1*

Table 6 presents results for the Au/HT3:1 catalyst in furfural oxidation for 2 (BR24) and 6 (BR36) hours of reaction**.** The results show a good trend in terms of furfural conversion. The selectivity to furoic acid and the carbon balance are a little bit lower after 6h of reaction and this means that the furfural and eventually the furoic acid suffer a bit from the degradation during the time of reaction.

7.5.3 Effect of the temperature of reaction on Au/HT activity

Table 7. Catalytic results at different temperatures for Au/HT3:1 catalyst

reaction	catalyst	T[°C]	X%	Y%	S%	c.b.%
BR24	Au/HT3:1	110	32,3	30,7	94,9	98,4
BR40	Au/HT3:1	130	52,6	34,8	66,1	82,2

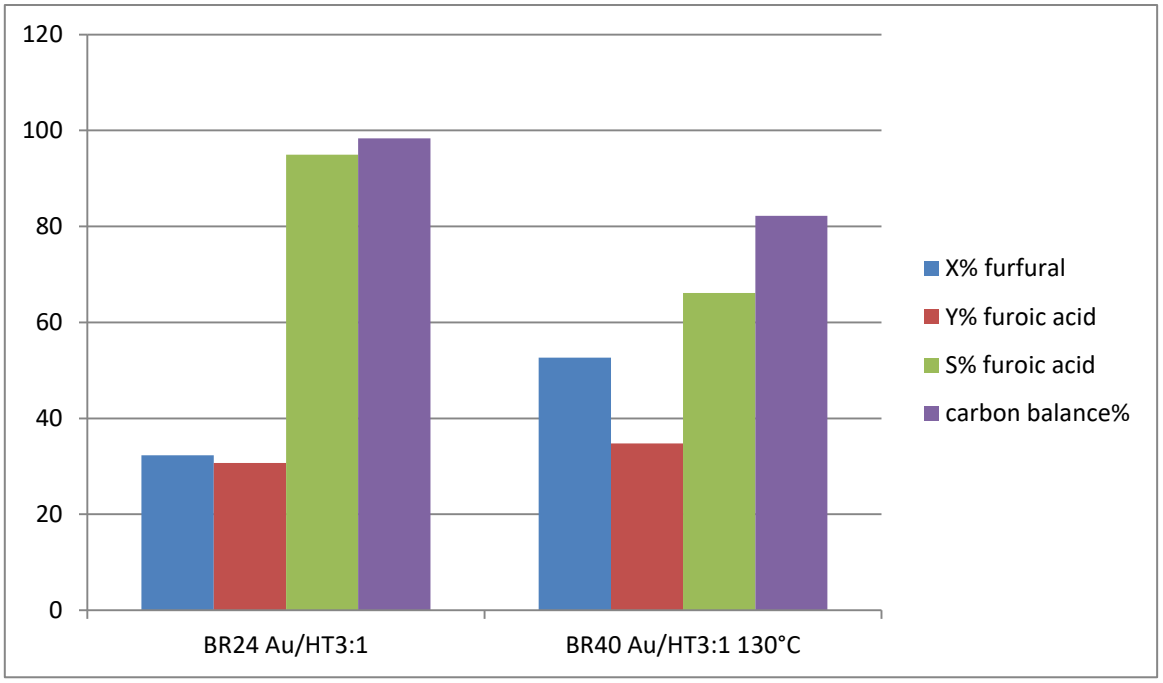

Figure 37. *Comparison between 2 different temperatures of reaction using Au/HT3:1*

The results in table 6 show clearly that at higher temperatures degradation of furfural occurs. Even if the conversion of furfural and better at higher temperature, the selectivity to furoic acid is much lower at 130°C than at 110°C (66% against 95%). The carbon balance decreases because some of the degradation products are probably formed which are not visible in HPLC. This reaction permitted to set up the final temperature of the reaction for other tests (110°C).

7.6 Catalytic oxidation of furfural on VPP based catalysts

After the tests with catalysts based on hydrotalcite it was decided to perform some tests with industrial catalyst: VPP made by Du Pont. VPP it is known to be a good oxidation catalyst to synthesize maleic acid from n-butane in gas phase process. Driven by curiosity, a test with this catalyst in standard conditions (50mg furfural, 20mL of water as solvent, 2 h as reaction time, 110°C as temperature, 6 bar of pressure and 900 rpm as stirring) and 100mg of VPP as catalyst was performed. The result is given on Figure 38.

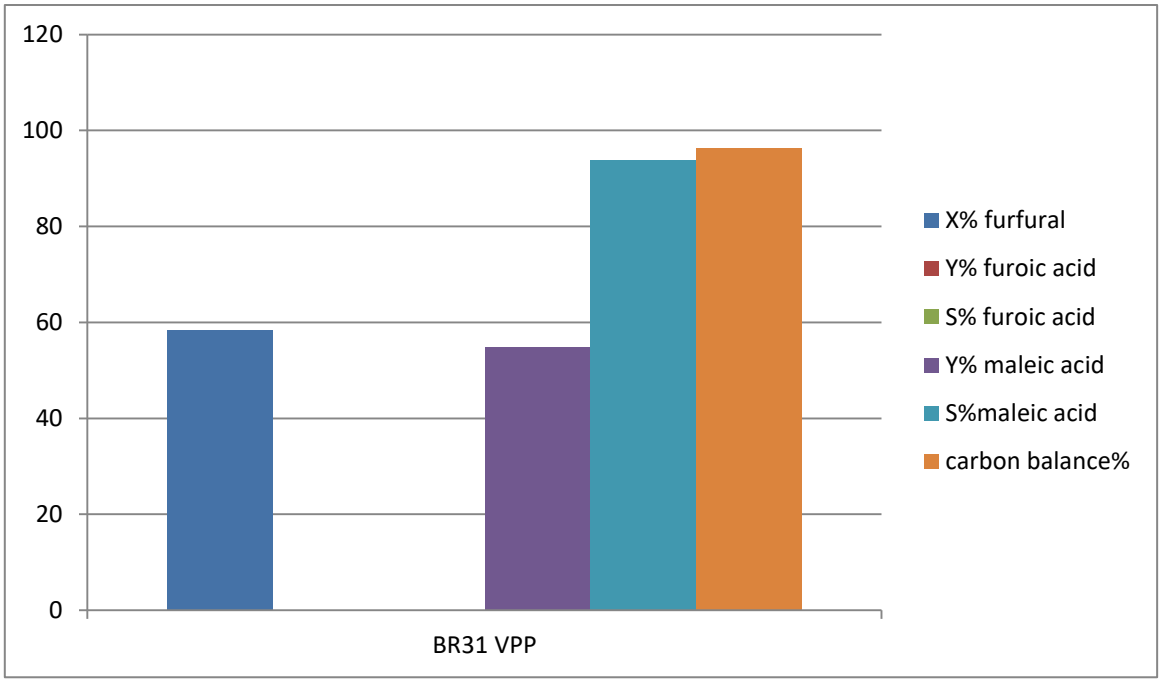

Figure 38. *Furfural oxidation on VPP catalyst*

Interestingly, in the case of the VPP catalyst there is no furoic acid formation from furfural. The HPLC spectra showed only one peak with the retention time corresponding to the maleic acid. This means that VPP catalyst changes completely the selectivity furfural in oxidative conditions. Taking this into account the calibration for maleic acid was made.

The reaction reaches almost 100% selectivity to maleic acid with a very good carbon balance.

This was a very interesting and unexpected result that drives the further study to deeper analysis of VPP catalyst in oxidation of furfural, used alone or also as a support for nanoparticles.

7.6.1 Effect of the time of reaction on VPP activity

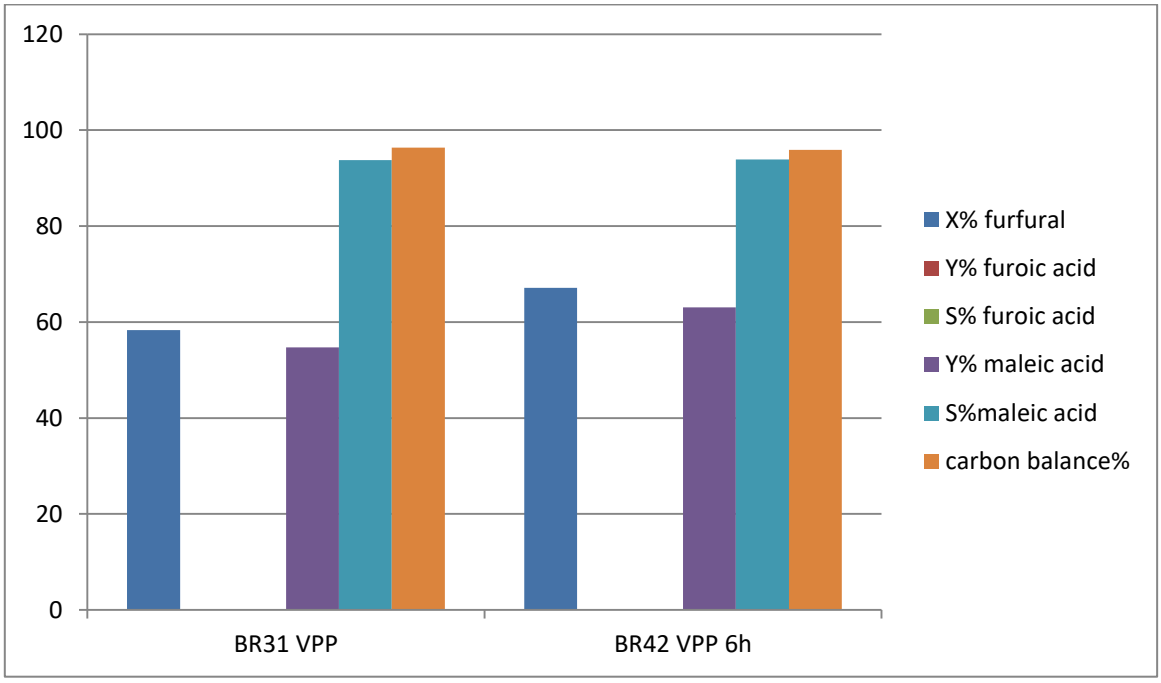

Figure 39. *Comparison between 2 different times of reaction using VPP catalyst*

Table 8. *Effect of time on catalytic activity of the VPP catalyst*

reaction	catalyst	t[h]	X%	Y%	S%	c.b.%
BR31	VPP	2	58,3	54,7	93,8	96,4
BR42	VPP	6	67,1	63,0	93,9	95,9

As could be seen from Table 8, the overall conversion increases with the time of the reaction. After 6 hours of the reaction the conversion reached almost 70% with very high selectivity (94%) to maleic acid. This result is very promising with the aim to develop an industrial process on this reaction with the possibility to reach high conversions without any problems due to the secondary reactions and a loss in terms of the selectivity and carbon balance.

7.6.2 Effect of the temperature of reaction on VPP activity

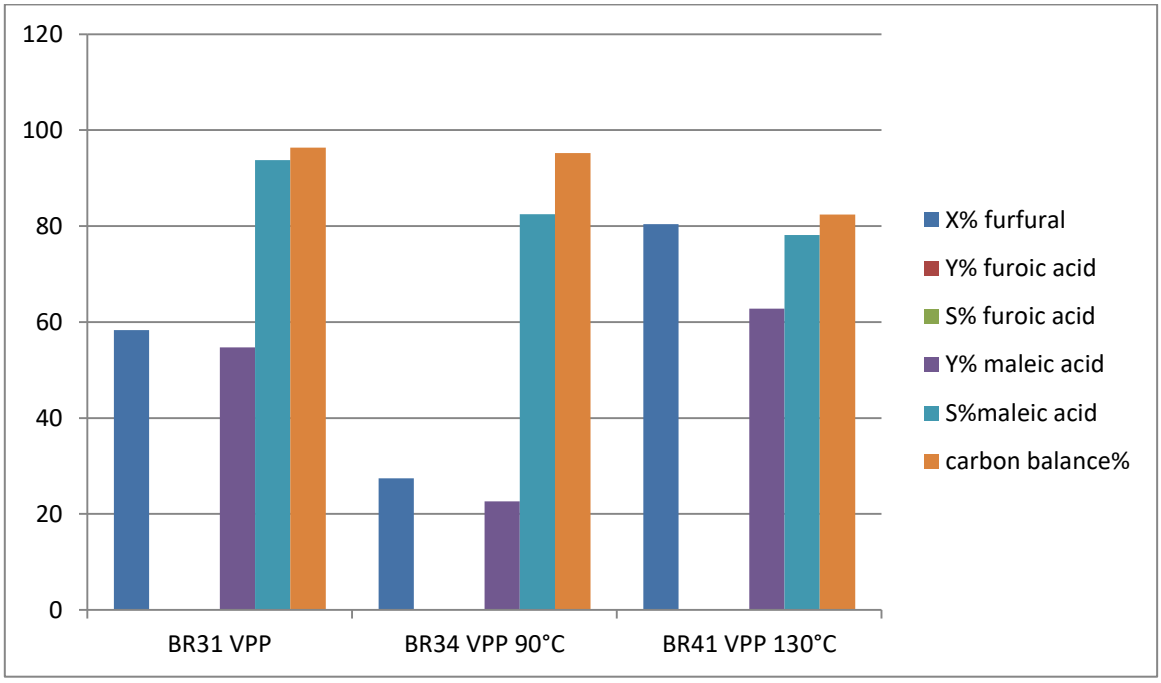

Figure 40. *Comparison between 3 different temperatures of reaction using VPP catalyst*

Table 9. Effect of the temperature on catalytic activity of VPP catalysts

reaction	catalyst	T[°C]	X%	Y%	S%	c.b.%
BR34	VPP	90	27,4	22,6	82,5	95,2
BR31	VPP	110	58,3	54,7	93,8	96,4
BR41	VPP	130	80,4	62,8	78,1	82,4

In the case of VPP catalysts the temperature of the reaction seems to play a crucial role, much more than in the case of the HT based catalysts, as can be seen from Figure 40. The higher temperature (130°C) provides a not negligible degradation of the furfural and/or products and the carbon balance is very low. Contrary to that, low temperature (90°C) of the reaction does not permit to obtain high conversion value (27,4%) without any gain in terms of the selectivity and carbon balance. The best temperature range for this reaction using VPP catalysts is 100-110°C. In this mid-range, the conversion is acceptable (almost 60%) and the selectivity is very high (94%).

7.6.3 Effect of the gold addition on the VPP catalyst activity

After the first good results with VPP catalyst it was decided to use VPP as a support for gold nanoparticles in the same way as for HT support. Generally it is well know that small gold nanoparticles permit to obtain high conversion even in low temperature. The results are given in Figure 41 and Table 10.

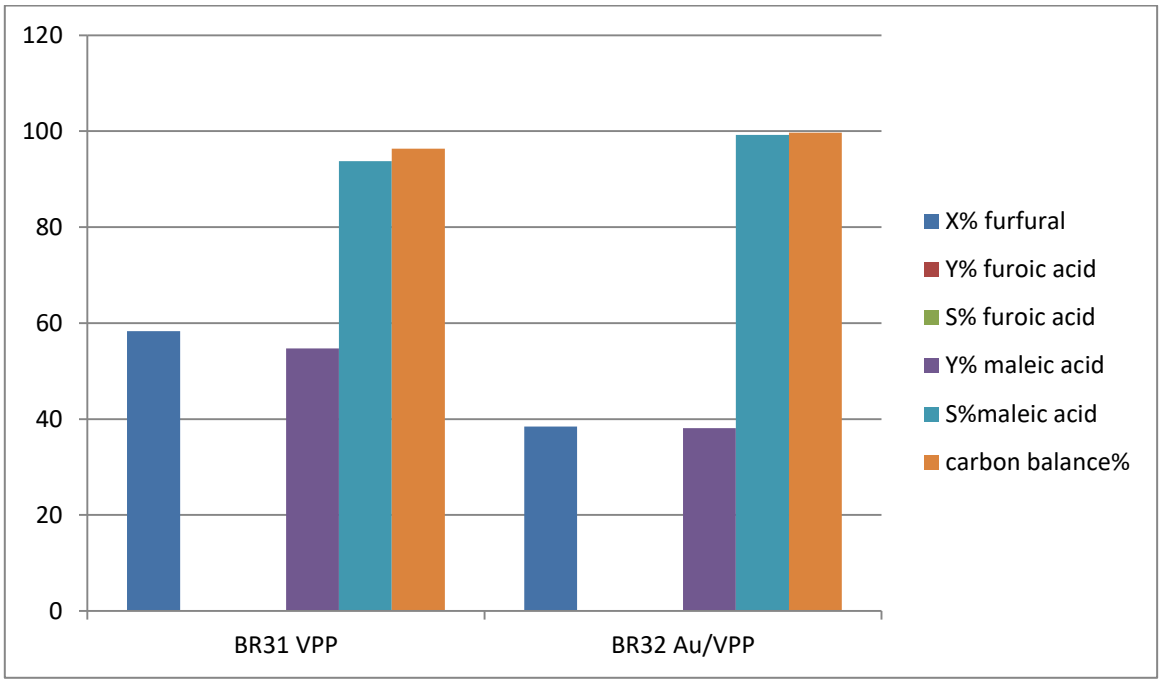

Figure 41. *Comparison between VPP and Au/VPP catalysts.*

Table 10. Effect of gold on catalytic activity of VPP catalyst

reaction	catalyst	X%	Y%	S%	c.b.%
BR31	VPP	58,3	54,7	93,8	96,4
BR32	Au/VPP	38,4	38,1	99,2	99,7

The results obtained with Au/VPP catalyst show a decrease of the overall activity of the catalyst if compared with bare VPP sample (Figure 41). This result was quite unexpected because the gold nanoparticles showed, in this case, negative effect on the catalyst activity. However, as expected (due to the lower conversion), the selectivity to final product is higher. However, these two catalysts give rise to several questions that should be study in the future with the aim to optimize this reaction.

The most important is to study the mechanism of the reaction, recyclability and stability of the catalysts. Especially the presence of leaching of the active phase should be confirmed (ICP study in progress).

7.7 5-Methylfurfural oxidation

Another part of this work was related to the reactivity of the 5-methyl furfural. This organic substrate is related to furfural and has similar chemical proprieties. Due to this reason very similar results were expected using similar conditions. The only structural difference is made by the methyl attached to the organic ring in position 5. This permits to obtain a 5-methyl furoic acid, which is one of the important chemical intermediates. Also, due to the methyl group, lower activity is expected for this reagent. Another problem linked to the 5-methyl furfural is that is not easy to solubilize it in water so an addiction of another solvent was used for this purpose.
The results of tests done with 5-methylfurfural are reported below.

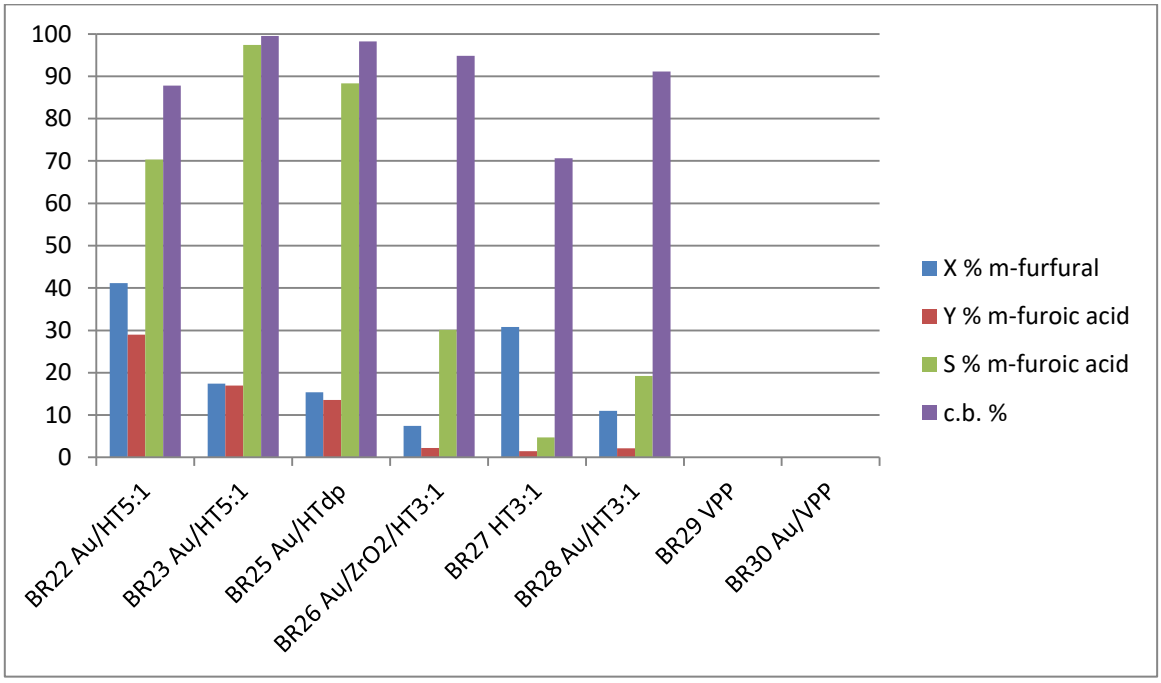

Figure 42. *5-methylfurfural oxidation to 5-methylfuroic acid*

As expected, 5-methylfuroic acid was the main product in all cases. The first test (BR22 on Figures 42 and 43) was made in the following conditions: 50mg 5-methyl

furfural, 19mL of water and one of ethanol as solvent, 2 h as reaction time, 110°C as temperature, 6 bar O_2 pressure and 900 rpm as stirring. The second one (BR23 in Fig. 43) has almost the same experimental conditions but 1 mL of acetonitrile was used instead of ethanol to solubilize the 5-methyl furfural. It is worth to note that these tests were performed only for 2 hours.

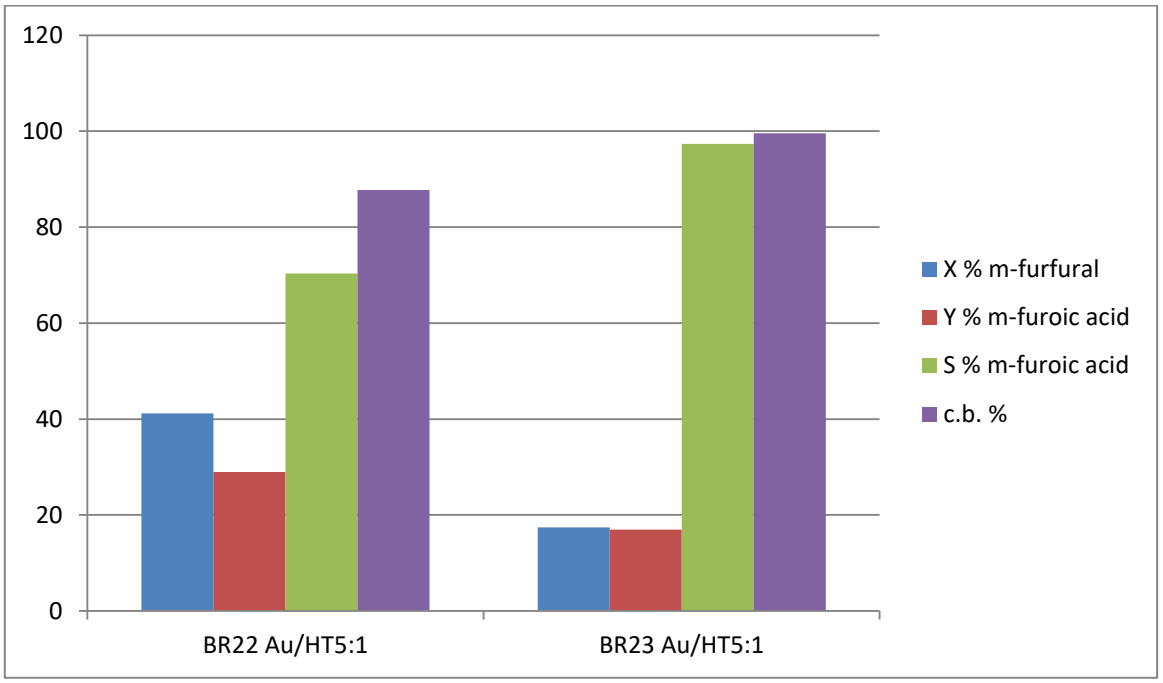

Figure 43. *Comparison between ethanol and acetonitrile as solvent additive*

BR22 shows good activity in terms of conversion and selectivity to 5-methylfuroic acid. However, the carbon balance reached only 90% (maybe due to the ethanol used for the sample preparation). With acetonitrile the carbon balance and the selectivity are much better (BR23). However, in this case the conversion is much lower. Due to the fact that ethanol can eventually undergo to esterification processes with acids and that this could be the reason of lower carbon balance, it was decided to proceed without it. Instead of that acetonitrile was used for further study despite the fact that the activity seems to be unfavourably influenced. BR25 and the following tests were made with the same condition as BR23 but with different catalysts. In particular, for

BR25, Au/HT_{DP} catalyst was used (DP corresponds to the method of preparation of this catalyst-precipitation) showed good activity, similar to that of Au/HT5:1 sample. The Au/HT3:1 catalyst, used in experiment BR28, showed much lower activity than BR23 which could be due to lower basicity of this material as compared to the Au/HT5:1. Moreover, gold nanoparticles were smaller also in the case of HT5:1 samples (please see TEM images).

7.7.1 5-methylfurfural oxidation on VPP catalysts

BR27 shows different results because the concentration of 5-methylfuroic acid produced is very low but other peaks in the HPLC chromatogram appear.

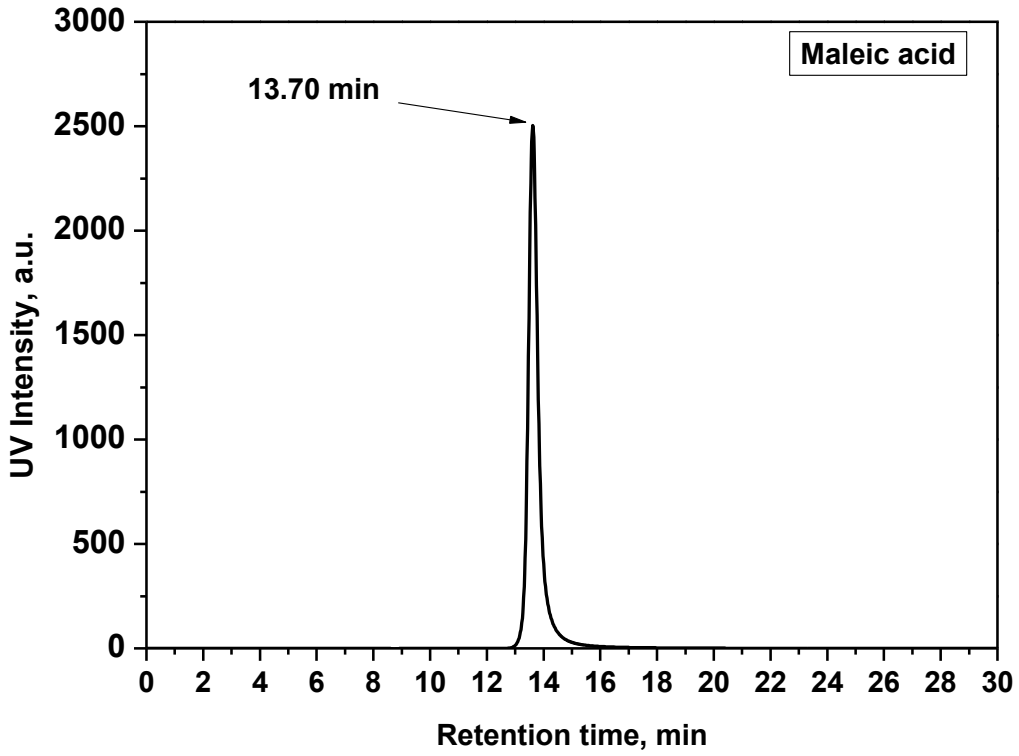

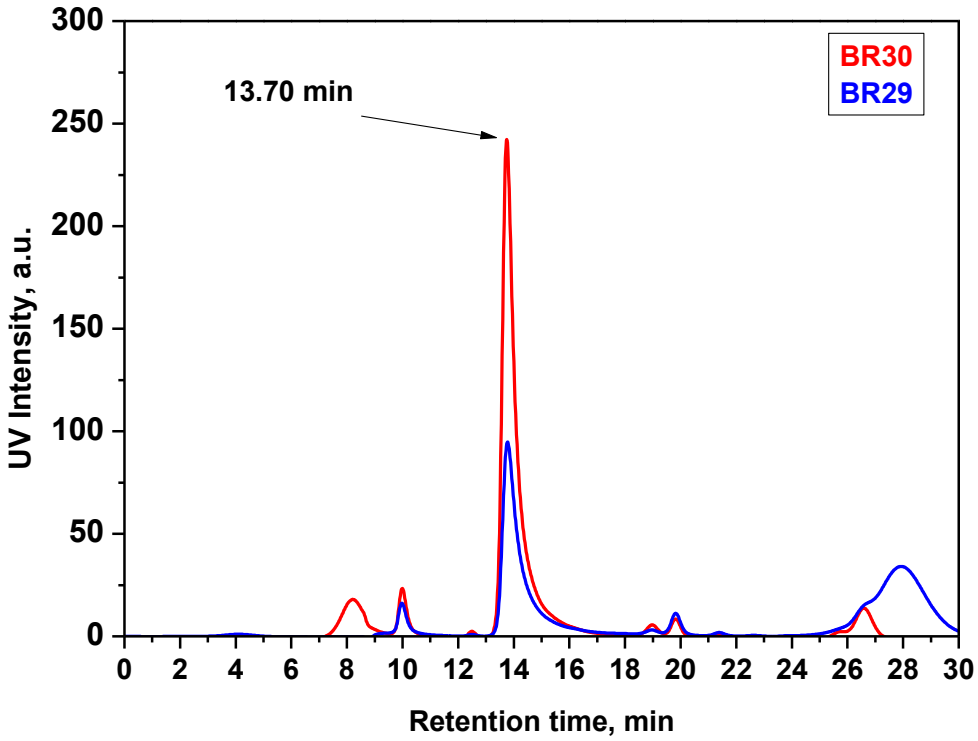

Figure 44. *HPLC chromatograms of the maleic acid (above) and experiments BR29 and BR30 (below)*

In BR29 and BR30 experiments (Figure 44) the retention time of the products correspond to the retention time of maleic acid. The conversion was total but only traces of methyl furoic acid were detected. NMR analysis is in progress to confirm the product.

7.8 Conditions on catalytic oxidation of 5-methylfurfural

After the screening of the catalytic materials it was decided to study the influence of different conditions of the reaction: time, temperature and 5-methylfurfural concentration in order to find the best conditions for the 5-methyl furoic acid synthesis.

These tests were made using Au/HT5:1 catalyst because it showed the best results in terms of conversion and yield (as described above).

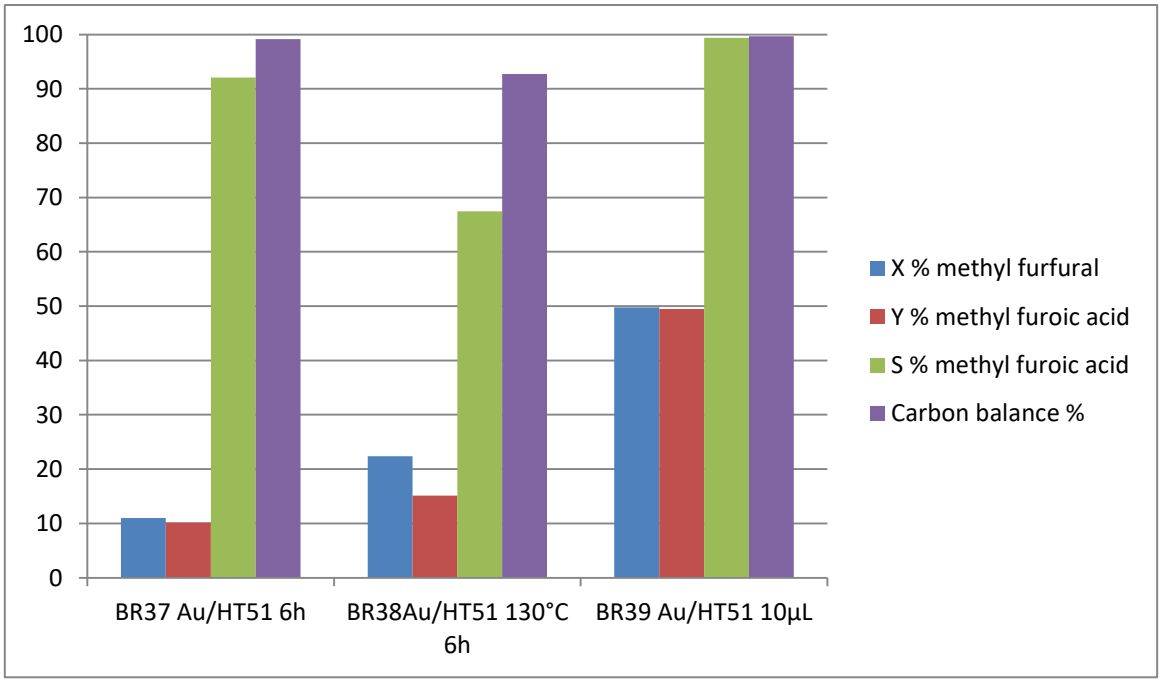

Figure 45. *Oxidation of 5-methylfurfural operative conditions modulation*

7.8.1 Effect of the time of reaction on Au/HT activity

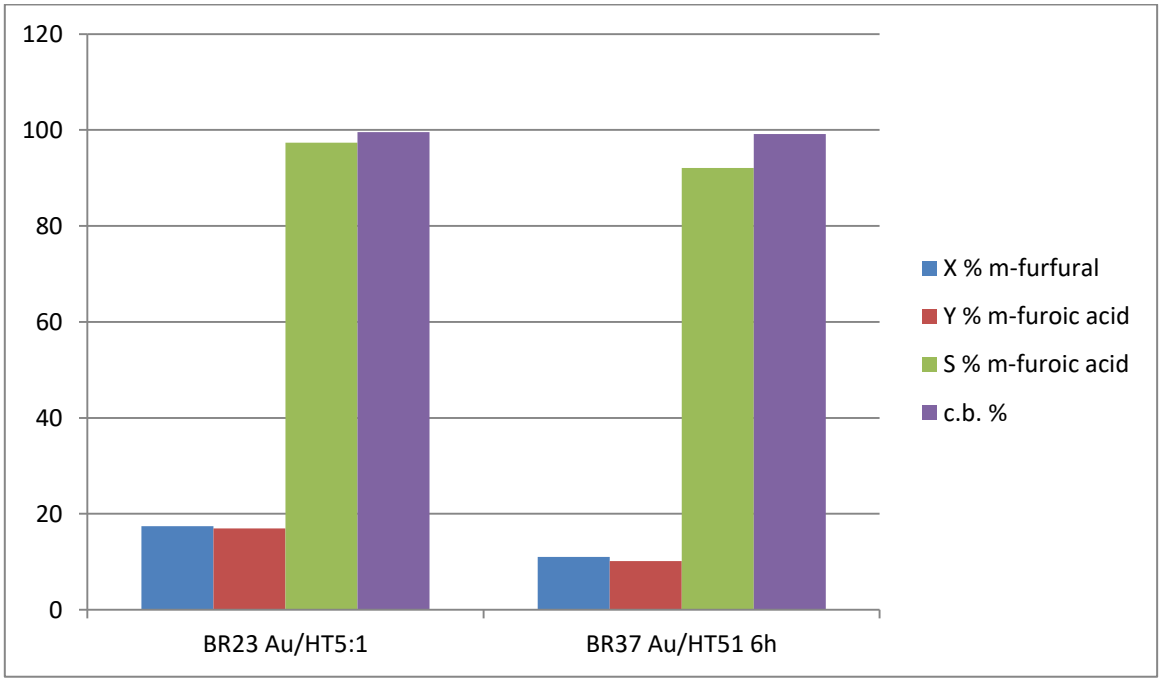

Figure 46. *Comparison between 2 different times of reaction with Au/HT5:1*

Table 11. Influence of time on catalytic activity of HT catalyst

reaction	catalyst	t[h]	X%	Y%	S%	c.b.%
BR23	Au/HT5:1	2	17,4	16,9	97,4	99,5
BR37	Au/HT5:1	6	11,0	10,1	92,1	99,1

Interesting results were observed in the study of the time of reaction. As could be seen from Table 11. The conversion after 6 hours of reaction is almost the same as after 2 hours of the reaction and carbon balance remained stable. It could be explained by the fast deactivation of the catalyst due to the adsorption of products on the catalysts surface and deactivation of the active phase. This hypothesis can be confirmed by performing tests with lower concentration of the substrate (results presented below).

7.8.2 Effect of the reagent concentration on Au/HT activity

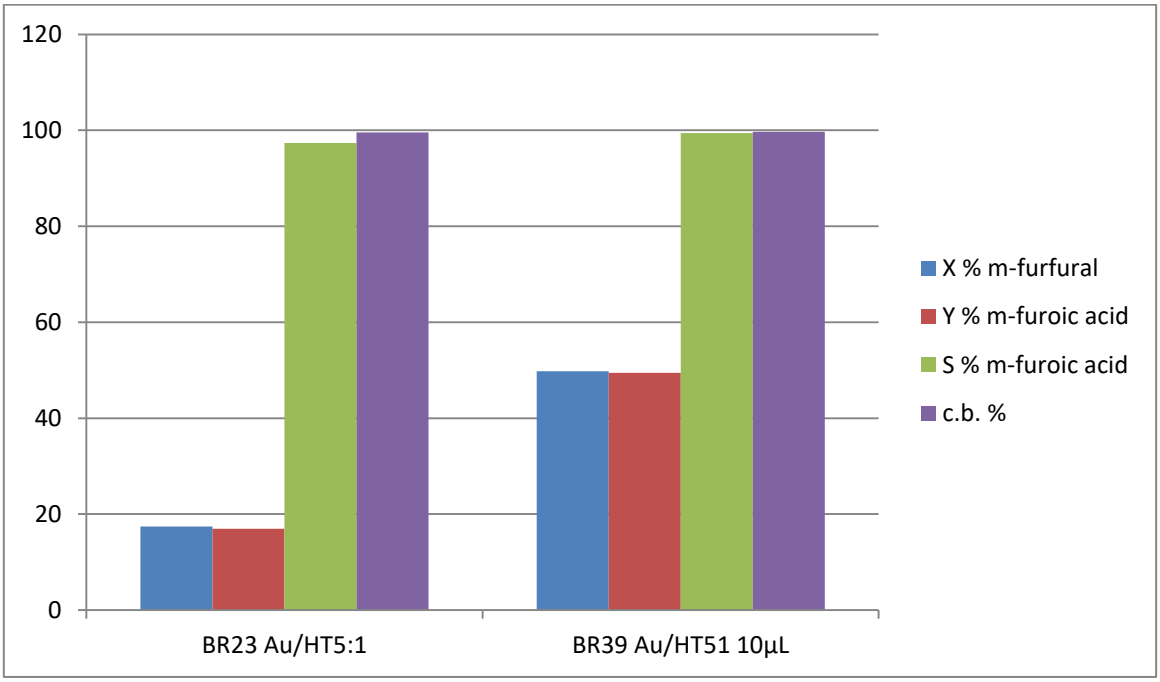

Figure 47. *Comparison between 2 different reagent concentrations for the reaction with Au/HT5:1*

Table 12. The effect of the reagent concentration on catalytic activity of the HT catalyst

reaction	catalyst	M reagent	X%	Y%	S%	c.b.%
BR23	Au/HT5:1	50mg	17,4	16,9	97,4	99,5
BR39	Au/HT5:1	11mg	49,8	49,5	99,4	99,7

This test was performed in order to check the influence of the substrate concentration on catalytic activity of the catalyst. It permitted also to check if the adsorption on the catalyst surface could be responsible for the suppression of the activity of the catalyst (please see above). A lower amount of the reagent would not deactivate all active sites of the catalyst, which would increase the activity of the catalyst.

As expected the activity was much higher and a very good selectivity was obtained. Due to lack of time, however, it was not possible to perform the same test using low reagent concentration but for 6h.

7.8.3 Effect of the temperature on Au/HT activity

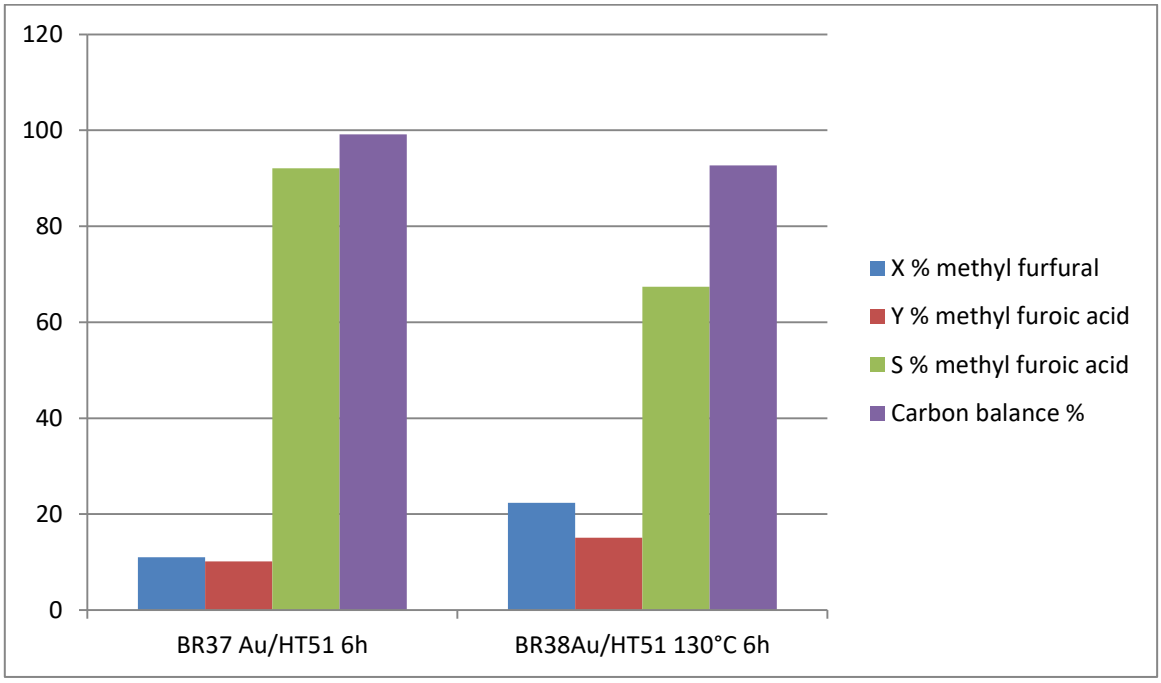

Figure 48. *Comparison between 2 different temperatures of reaction with Au/HT5:1*

Table 13. Influence of the temperature on catalytic activity of the HT catalysts

reaction	catalyst	T[°C]	X%	Y%	S%	c.b.%
BR37	Au/HT5:1	110	11,0	10,1	92,1	99,1
BR38	Au/HT5:1	130	22,4	15,1	67,4	92,7

As a general trend the results are comparable with that observed for furfural. High temperature permits to increase the conversion but at the same time the selectivity decreases significantly. The carbon balance due to the degradation is lower at high temperature. As in the case with furfural, the 100-110°C temperature range seems to be optimal (Figure 48) for these type of materials keeping good compromise between conversion, selectivity and carbon balance.

CONCLUSIONS

The aim of this master thesis was to investigate the oxidation of furfural and 5-methylfurfural in green condition, using oxygen and heterogeneous catalysts. These two reagents are considered green because they are derived from biomass, in particular hemicellulose, and this factor makes the overall process of great interest. Due to the fact that both reagents are not very stable in water, at first a biphasic system composed of water and of organic solvent (MBIK) was tested. Some tests were performed but unfortunately the problems with analyse of the products appeared (products degradation). The general idea of the biphasic system utilization is very interesting because of the use of organic phase as furfural storage and the reaction occurs in water phase. This should be study in the next future.

After this point the research was reoriented to tests using water as solvent and different types of catalysts. Moreover, two important substrates were studied: furfural and 5-methylfurfural. The products obtained were mainly furoic acid (from furfural) and 5-methylfuroic acid (from 5-methylfurfural). These compounds are very interesting in many fields and they were obtained with a very good selectivity (and good carbon balance). The best catalyst for this reaction was Au nanoparticles supported on hydrotalcite synthesised with the Mg/Al ratio of 5. The conversion of furfural was always higher than that of 5-methylfurfural, probably due to the presence of the methyl group.

Very interesting results were obtained with an industrial vanadyl pyrophosphate (VPP) catalyst. It showed a very good activity when compared to HT based catalysts. And surprisingly in this case formation of furoic acid was not observed. Instead of that a good selectivity to maleic acid was observed with relatively good conversion. Maleic acid is a very important molecule and the target molecule at the beginning of the study. This result is one of the most important achievements of this thesis and makes this study particular interesting from the industrial point of view.

Following these good catalytic results the characterization of the most active catalysts was made. The characterization was done using different analytical techniques: X-ray diffraction, X-ray fluorescence and Scanning and Transmission Electron Microscopy.
To finish the reaction conditions for two catalysts were studied: temperature, pressure, time and substrate concentration.
The best condition for the production of furoic acid are: temperature of 100-110°C, 15 bar of oxygen and Au/HT catalyst with the Mg/Al ratio of 5. In case of the methyl furfural oxidation the same conditions could be used yielding good quantity of 5-methylfuroic acid on Au/HT catalysts.
In case of the maleic acid production VPP based catalysts need to be used but the conditions could be the same as for the Au/HT materials. Also a gold modified VPP catalyst was tested but it resulted in a lower selectivity to maleic acid (at higher conversion).
Further studies should be carried out in the aim to improve the catalytic system, mainly for the synthesis of the maleic acid. New catalysts could be prepared based on the industrial VPP catalyst and study of the biphasic system should continue.

REFERENCES

[1] H. Guo and G. Yin, *Catalytic Aerobic Oxidation of Renewable Furfural with Phosphomolybdic Acid Catalyst: an Alternative Route to Maleic Acid*; J. Phys. Chem. C, **2011**, 115 (35), pp 17516–17522

[2] B. Kamm, P. Gruber, M. Kamm, *Biorefineries-Industrial Processes and Products: Status Quo and Future Directions*; vols.1 and 2, Wiley-VCH, Weinheim, **2005**.

[3] H.Z. Chen. *Ecological high value-added theory and application of crop straws*. Beijing: Chemical Industry Press; **2006**.

[4] S.H. Yang, *Plant fiber chemistry*. Beijing: China Light Industry Press; **2008**

[5] J.Q. Zhang, L. Lin, Y. Sun, G. Mitchell, S.J. Liu. *Advance of studies on structure and decrystallization of cellulose*. Chem Ind For Prod. **2008**; 28(6):109–14.

[6] P. Zhang, H.R. Hu, S.L. Shi. *Application of hemicellulose*. Tianjin Pap Mak. **2006**; 2:16–8.

[7] G. Burdok, *Encyclopedia of Food & Color Additives* **1996**, "P-Z indexes; Boob Stern p.2359.ISBN0-8493-9414-7

[8] T.D. Jiang, *Lignin*. Beijing: Chemical Industry Press; **2001**.

[9] J.H. Wei, Y. R. Song. *Recent advances in study of lignin biosynthesis and manipulation*. J Integr Plant Biol. **2001**; 43(8):771–9.

[10] J. Gao, L.G. Tang. *Cellulose science*. Beijing: Science Press; **1996**

[11] W. M. Van Rhijn, W. Van Rhijn, D. E. De Vos, P. A. Jacobs, H. E. Hoydonckx, *Furfural and Derivatives*; Ullmann's Encyclopedia of Industrial Chemistry

[12] R. Adams and V.Voorhees; *Furfural*. Org. Synth. Coll 1921, 1:49;. Vol.1 pag 280;

[13] https://en.wikipedia.org/wiki/Furfural

[14] R. Wojcieszak, F. Santarelli, S. Paul, F. Dumeignil, F. Cavani, R. Gonçakves, *Recent developments in maleic acid synthesis from bio-based chemicals*; Sustain Chem Process (**2015**) *3:9*

[15] G. Burdok, *Encyclopedia of Food & Color Additives* **1996**, "P-Z indexes; Boob Stern p.2359.ISBN0-8493-9414-7

[16] Dr. Weiran Yang, Prof. Ayusman Sen; *Direct Catalytic Synthesis of 5-Methylfurfural from Biomass-Derived Carbohydrates*; 26 January **2011**; 10.1002/cssc.201000369

[17] A.Cahana, J.Standiford, P.Mikochik, WO2014046982 A1

[18] D. Martin Alonso, J. Q. Bond and J. A. Dumesic; Catalyt*ic conversion of biomass to biofuels*; Green Chem., **2010**,12, 1493-1513;

[19] S. Shi, H. Guo, G. Yin; *Synthesis of maleic acid from renewable resources: Catalytic oxidation of furfural in liquid media with dioxygen*. Catal. Comm. **2011,** 12, 731-733

[20] P. Beltrame et al. Applied Catalysis A: General 297 (2006) 1–7

[21] M. Comotti, C. Della Pina, R. Matarrese, M. Rossi, Angew. Chem. Int. Ed. 43 (2004) 5812.

[22] S. Biella, L. Prati, M. Rossi, J. Catal. 206 (2002) 242.

[23] C. Baatz et al. Applied Catalysis B: Environmental 70 (2007) 653–660

[24] Y. Onal, S. Schimpf, P. Claus, J. Catal. 223 (2004) 122

[25] T. Benkó et al. Applied Catalysis A: General *388 (2010) 31–36*

[26] A. Stephen, K. Hashmi, Chem. Rev. 107 (2007) 3180–3211.

[27] P. Beltrame, M. Comotti, C. Della Pina, M. Rossi, J. Catal. 228 (2004) 282–287.

[28] T. Ishida, N. Kinoshita, H. Okatsu, T. Akita, T. Takei, M. Haruta, Angew. Chem. Int. Ed. 47 (2008) 9265–9268.

[29]] H. Okatsu, N. Kinoshita, T. Akita, T. Ishida, M. Haruta, Appl. Catal. A 369 (2009) 8–14.

[30] D. Huang; F. Liao; S. Molesa; D. Redinger; V. Subramanian. Journal of the Electrochemical Society, **2003**, 150, G412-417

[31] T. Stuchinskaya; M. Moreno; M. Cook, D. Edwards, D. Russell, Photochem. Photobiol. Sci., **2011**, 10, 822-831

[32] S. D. Brown, P. Nativo, J.A. Smith; D. Stirling, P.R. Edwards, B. Venugopal, D.J. Flint, J.A. Plumb, D. Graham, N.J. Wheate, J. Am. Chem. Soc., **2010**, 132, 4678-4684

[33] S. Perrault, W. Chan, Proc. Nat. Acad. Sci. USA, **2010**, 107, 11194-11199.

[34] G. Peng, U. Tisch, O. Adams, M. Hakim, N. Shehada, Y. Broza, S. Bilan, R. Abdah-Bortnyak, A. Kuten, H. Haick, Nature Nanotech., **2009**, 4, 669-673

[35] D. T. Thompson, Nano Today, **2007**, 2, 40-43

[36] T. Ishida,N. Kinoshita, H. Okatsu, T. Akita, T. Takei, M. Haruta, M.; *Influence of the Support and the Size of Gold Clusters on Catalytic Activity for Glucose Oxidation*, Ang. Chem. Inter. Ed., **2008**, 47, 9265-9268

[37] M.J. Hudson and J.A. Knowles, *Preparation and characterisation of mesoporous, high-surface-area Zirconium (V) oxide,* J. Mater. Chem. **1996**, 6 (1), 89-95

[38] http://www.bris.ac.uk/nerclsmsf/techniques/gcms.html, 11/09/2016

[39] https://xos.com/technologies/xrd/, 11/09/**2016**

[40] https://xos.com/technologies/xrf/, 11/09/**2016**

[41] http://serc.carleton.edu/research_education/geochemsheets/techniques/SEM.html

[42] PhD thesis of G. Pavarelli. University of Bologna, Italia, **2009**

[43] N. F. Dummer, W. Weng, K.Kiely, A. Carley, J. Bartley, Ch. Kiely, G. Hutchings, Appl. Catal. A: General 376 (**2010**) 47-55